Universiteit
Leiden
The Netherlands

# Novel analytical approaches for the characterization of cell-based medicinal products and their formulation

Rösch, A.

**Citation**
Rösch, A. (2025, June 10). *Novel analytical approaches for the characterization of cell-based medicinal products and their formulation*. Retrieved from https://hdl.handle.net/1887/4249627

| | |
|---|---|
| Version: | Publisher's Version |
| License: | Licence agreement concerning inclusion of doctoral thesis in the Institutional Repository of the University of Leiden |
| Downloaded from: | https://hdl.handle.net/1887/4249627 |

**Note:** To cite this publication please use the final published version (if applicable).

# CHAPTER 2

## Particles in biopharmaceutical formulations, part 2: An update on analytical techniques and applications for therapeutic proteins, viruses, vaccines and cells

Alexandra Roesch[1,3], Sarah Zölls[1], Daniela Stadler[1], Constanze Helbig[1], Klaus Wuchner[2], Gideon Kersten[1,3], Andrea Hawe[1], Wim Jiskoot[1,3,†], Tim Menzen[1*]

[1] Coriolis Pharma, Fraunhoferstr. 18 b, 82152 Martinsried, Germany

[2] Janssen Research and Development, DPD&S Biotherapeutics Development, Hochstr. 201, 8200 Schaffhausen, Switzerland

[3] Leiden Academic Centre for Drug Research (LACDR), Leiden University, PO Box 9502, 2300, RA, Leiden, The Netherlands

*corresponding author

† In memoriam of Prof. Dr. Wim Jiskoot, our valued colleague, who passed away unexpectedly during writing of this review article.

The chapter was published in the *Journal of Pharmaceutical Sciences: J Pharm Sci 2022;111(4):933–950.*

## Abstract

Particles in biopharmaceutical formulations remain a hot topic in drug product development. With new product classes emerging it is crucial to discriminate particulate active pharmaceutical ingredients from particulate impurities. Technical improvements, new analytical developments and emerging tools (e.g., machine learning tools) increase the amount of information generated for particles. For a proper interpretation and judgment of the generated data a thorough understanding of the measurement principle, suitable application fields and potential limitations and pitfalls is required. Our review provides a comprehensive overview of novel particle analysis techniques emerging in the last decade for particulate impurities in therapeutic protein formulations (protein-related, excipient-related and primary packaging material-related), as well as particulate biopharmaceutical formulations (virus particles, virus-like particles, lipid nanoparticles and cell-based medicinal products). In addition, we review the literature on applications, describe specific analytical approaches and illustrate advantages and drawbacks of currently available techniques for particulate biopharmaceutical formulations.

## Introduction

Biopharmaceuticals, such as therapeutic proteins, vaccines, as well as gene and cell therapy products, remain an increasing field in the pharmaceutical industry with numerous approved treatments and ongoing clinical trials [1, 2]. A key aspect in drug product development is particle analysis. In order to establish meaningful particle analysis methods for biopharmaceuticals, it is of high relevance to define what is considered "a particle". In Table 1 we made an attempt to provide definitions depending on the context of biopharmaceutical product and/or scope of analysis. For protein-based therapeutics, aggregates larger than 0.1 µm are defined as particles [3], whereas for particulate delivery systems the delivery vehicle, cell or virus themselves are particles.

*Table 1: Definitions of particle types in different (bio)pharmaceutical contexts.*

| (Bio)pharmaceutical context | Particle types and definition |
|---|---|
| Therapeutic proteins: aggregates and particles | There is no clear threshold at which size a protein aggregate is considered a "protein particle". In the biopharmaceutical industry, the definition from Narhi et al.[3] is most often used:<br>● 10-100 nm: Protein oligomers<br>● 0.1-1 µm: Sub-micrometer particles/ nanometer aggregates<br>● 1-100 µm: Subvisible particles/ micrometer aggregates<br>● > ~ 100 µm: Visible particles<br>The differentiation between soluble and insoluble aggregates is obsolete, because the definition of "solubility" depends on the method used to assess "soluble" aggregate content. The size limit for visible particles, related to likelihood of detection, depends on many factors (e.g., particle quantity, size, shape, color, density, and reflectivity, translucency), and is usually well above 100 µm for protein (translucent) particles. |
| Viruses and virus like particles (VLP) | Viruses and VLP are typically referred to as (nano)particles; liquid virus and VLP formulations are called suspensions or dispersions. |
| Particulate delivery systems (e.g., lipid nanoparticles, lipoplexes, polymer-based nano- and microparticles) | Particulate delivery systems are typically referred to as (nano- or micro)particles; particulate delivery systems in a liquid formulation are suspensions or dispersions. |
| Cell-based medicinal products (CBMPs) | CBMPs in a liquid formulation are typically referred to as cell suspensions or dispersions, which means that a cell is a (micro)particle. |
| Extrinsic, intrinsic and inherent particulate impurities as outlined in USP<1787> and USP<1790> | **Extrinsic particles** are not part of the formulation, package, or assembly process and may originate from:<br>● Biological external sources (e.g., insect parts, pollens, vegetative matter)<br>● Building materials (e.g., non-process-related fibers, lint, minerals, paint)<br>● Personnel (e.g., epithelial cells, clothing fragments, hairs) |

**Intrinsic particles** derive from sources within the formulation ingredients, assembly process, or primary packaging materials, due to:

● Introduction during processing or not completely removed during cleaning and preparation (e.g., elastomers from seals and gaskets, container plastic or glass shards, stainless steel parts)

● Lubricants of primary packaging components (e.g. silicone oil in siliconized syringes)

● Changes in the drug product over time, which may be related to ionic or organic extracts (e.g., leachables from rubber stoppers), instability of the active pharmaceutical ingredient (e.g., unexpected subvisible and visible protein particles), excipient degradation (e.g., fatty acid particles from degraded polysorbate), or product–package interaction (e.g., glass delamination).

**Inherent particles** are intentionally present or expected including solutions, suspensions, emulsions, and other drug delivery systems that are designed as particle assemblies (agglomerates, aggregates), e.g.:

● Virus, virus-like particles, lipid nanoparticles, cells, other microparticulate formulations

● Product-formulation-related particles (e.g., proteinaceous aggregates or excipient-related degradation products such as fatty acid particles) characteristic of the product if their presence is measured, characterized, and determined to be part of the clinical profile.

In general, particles in a drug product must be closely monitored together with other critical quality attributes (CQAs), as they can compromise the product's quality and safety. During the development of protein therapeutics particle analysis is used during formulation development and stability testing to evaluate impact factors such as pH or excipients on protein aggregation [4–7]. In recent years the immunogenic potential of protein particles has increasingly moved into focus [8–12].

Particulate-based biopharmaceuticals include cell-based medicinal products (CBMP), virus particles, virus-like particles (VLP), inactivated and attenuated viruses, as well as lipid nanoparticles (LNP). CBMP are an emerging category of medicines offering treatment options for severe diseases, such as cancer, immunological disorders and genetic diseases [2]. In general, CBMP are living cells, which can be derived from autologous (patient's) or allogenic (healthy donor) material [13]. Viruses, beside their long-standing use in classical vaccination approaches, are applied increasingly as viral vectors for gene therapy [14], delivery vehicle for nucleic acid vaccines [15–17] or as oncolytic viruses in cancer therapy [18]. Viral vectors contain a recombinant viral genome bearing the therapeutic transgene for gene therapy and nucleic acid vaccines. Expression of the therapeutic gene can be transient or long term, depending on the viral vector [14, 19, 20]. Oncolytic viruses are designed to target and destroy tumor cells either directly or by

lysing tumor blood vessels and can additionally activate an antitumor immune response or deliver a therapeutic gene [18]. VLP are an important category of subunit vaccines, and they are also being developed as delivery system for drugs [21, 22]. VLP resemble viruses that enclose their genome in a protein capsid or in a phospholipid envelope, but they are devoid of genetic material and therefore non-infectious. LNP are nanoparticles used for delivery of nucleic acids such as siRNA and mRNA. They differ from liposomes (phospholipid bilayer nanoparticles with a liquid interior) in that they have a solid core filled with lipids plus the active molecules. Nucleic acids are surrounded by cationic or ionizable cationic lipids. Phospholipid and cholesterol (helper lipids) add structure to the solid core and the nanoparticles are stabilized by a monolayer of PEG-lipid conjugates. The exact structure of LNP may depend on lipid composition, type and concentration of the nucleic acid and preparation methods.

Due to the heterogeneity of biopharmaceuticals, as well as the purpose/scope of the analysis the selection of analytical techniques is of high relevance, and often several ideally orthogonal techniques need to be combined. In addition, the stages of drug product development require specific characteristics of analytical methods to assure a phase appropriate application [23]. The focus shifts from low sample consumption, high throughput, and automation capability during early development phases towards a method's stability-indicating properties, robustness, statistical relevance of results, and ease of use in regulated environments (quality control (QC)-friendliness) during late stage development and release testing. For release testing it is typically sufficient to focus on the CQAs, because the product is well characterized during development and appropriate control strategies are in place. As an example, for protein therapeutics, release testing typically includes oligomer analysis by SEC, turbidity (typically caused by submicron particles and/or effects related to reversible self-association), subvisible particle analysis by light obscuration (LO) and visual inspection for visible particles [23, 24]. Submicron particle methods are regularly applied for extended product characterization and troubleshooting; the reported relatively low robustness is an unmet challenge for application in QC [25–27]. Interlaboratory and cross-industry studies have become very valuable in demonstrating the performance and limitations of several particle techniques [25, 28–30]. The key is to choose the right method(s) for the right application at the right phase during product development.

This review is divided in two parts. Firstly, we give an update on analytical techniques and approaches, which have emerged in the last decade since our first review (Particles in therapeutic protein formulations, Part 1: overview of analytical methods) has been published in 2012 [31]. Secondly, we give a comprehensive overview of the application of particle analysis for the different types of biopharmaceuticals including therapeutic proteins and particulate biopharmaceutical formulations such as virus particles, VLP, LNP, and CBMP.

## An update on analytical techniques and tools for particle analysis

This section provides an overview of particle analysis techniques and tools that have emerged in the last decade and can be used as an extension to those techniques described by Zölls et al. [31]. Apart from the new techniques described below, some existing techniques have undergone technical improvements. For instance, a new LO instrument has become available, where the sample chamber can be pressurized, allowing the analysis of viscous samples and reducing the impact of air bubbles [32]. Autosamplers or liquid handling systems for flow imaging techniques have become commercially available.

Below, we provide general descriptions of new techniques, including measurement principles, output parameters, pros and cons, as well as application possibilities with a "track record" in the literature and biopharmaceutical industry. Figure 1 shows an overview of established and new techniques and their possible applications. For technical details and in depth explanations about the underlying measurement principles, the reader is referred to the review by Gross-Rother et al.[33] In addition, we cover the aspect of machine learning as emerging tool for image-based particle analysis in this section. Very recent techniques specific for nanoparticulate formulations will be discussed in the subsequent sections covering characterization of particulate biopharmaceutical formulations.

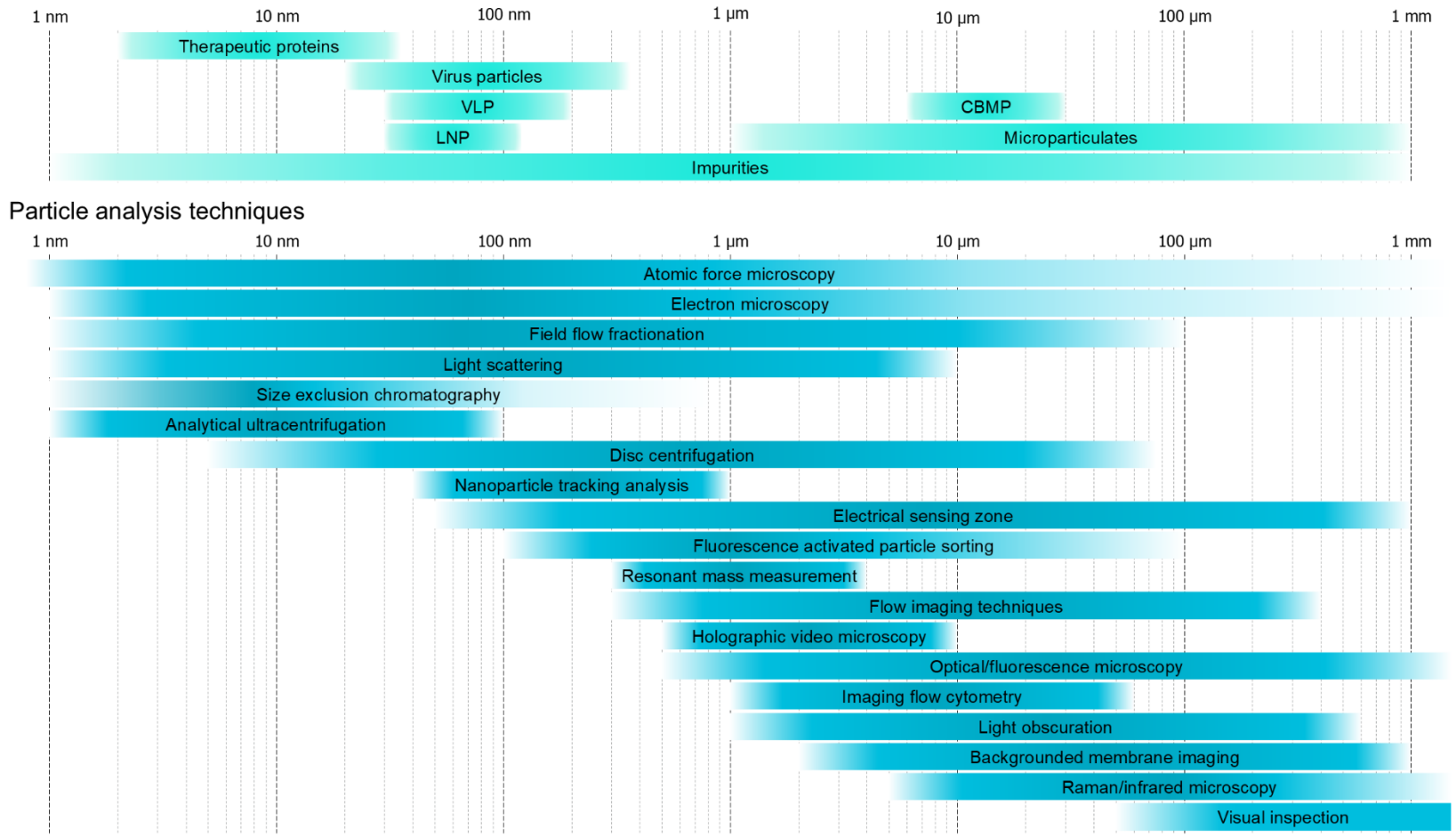


*Figure 1: Overview of the approximate size range of particles in biotherapeutics (turquois-blue) as well as applicable particle analysis techniques (dark blue). Field flow fractionation includes the techniques asymmetrical flow field-flow fractionation and hollow fiber flow-field-flow fractionation. Techniques/instruments based on the electrical sensing zone are Coulter counter, tunable resistive pulse sensing and microfluidic resistive pulse sensing. Visual inspection includes camera-based systems. Abbreviations: LNP: lipid nanoparticle; VLP: virus-like particle; CBMP: cell-based medicinal products.*

### Resonant mass measurement (RMM)

RMM reflects an analytical approach which is based on the frequency shift of a resonating cantilever (also known as suspended microchannel resonator (SMR)) proportional to the buoyant mass of particles floating past the cantilever [34]. The only system on the market so far is the Archimedes system developed by Affinity Biosensors in two generations, lastly marketed by Malvern Panalytical.

Particles with a higher density than the surrounding fluid decrease the frequency of the oscillating cantilever, whereas particles with lower density increase the frequency. This enables a straightforward discrimination between protein particles and silicone oil droplets based on their density[35–39] in a size range of the critical "submicron size gap"[40, 41] of approx. 0.3 to approx. 4 µm. Using an estimated density for protein particles (e.g., the density of pure protein of 1.32 g/cm$^3$ [42], or an experimentally determined density of 1.28 – 1.33 g/cm$^3$ [43]), a particle size distribution can be obtained for protein particles.The optimum concentration depends on the type of sample and was reported as 3x10$^5$ to 1x10$^7$ particles/mL [35] or 1x10$^6$ to 1x10$^9$ particles/mL [44].

Challenges of the technique include clogging of the very narrow sensor channel by larger particles, potential fragmentation of larger particles or droplets by shearing and shedding forces [35] and a high variability in results due to the very low analyzed volume. Reproducibility can be improved by rigorous protocols and best practice approaches [44].

### Electrical sensing zone/Coulter principle

Based on the electrical sensing zone, also known as Coulter principle[45], two variations have emerged: tunable resistive pulse sensing (TRPS) and microfluidic resistive pulse sensing (MRPS). Similar to the Coulter counter, sample solutions for both techniques must have a sufficient conductivity which needs in many cases the addition of salts [46]. TRPS and MRPS circumvent several drawbacks of the Coulter counter, such as a high sample consumption and the need for several apertures to cover a greater particle size range, thereby offering new possibilities for the analysis of biopharmaceuticals. TRPS uses an elastic pore, which can be stretched to measure particles between 50 nm and 20 µm, providing the opportunity to adapt the pore size depending upon the particles to be analyzed. Thereby, the blockage of the pore by stuck particles can be prevented. The required sampling volume is 40 µL, and the particle concentrations may range between 1x10$^5$ and 1x10$^{12}$ particles/mL. Within MRPS instruments disposable microfluidic cartridges containing a built-in filter to avoid blockage of the orifice are used. Several pore sizes are available to cover the size range from 50 to 2000 nm. Merely 3 µL sample volume is enough to analyze particle concentrations from 1x10$^6$ to 1x10$^{12}$ particles/mL.

The measurement principle of MRPS and TRPS is independent of light and therefore enables the detection of translucent particles that are difficult to detect via light-based techniques. As orthogonal

methods to light-based methods both techniques provide a valuable tool for particle characterization in the submicron and low-micron size range.

### Backgrounded membrane imaging (BMI)

BMI uses an automated 96-well plate-based approach for the microscopic analysis of particles in the size range above 2 µm. In brief, membrane filter well plates are imaged before and after sample application, and final particle images are obtained after background correction. This technique is currently implemented in the Horizon instrument (Halo Labs, Burlingame, CA), which covers an approximate concentration range between $1\times10^3$ and $7\times10^5$ particles/mL. Output parameters include particle size, shape and morphology parameters (e.g., equivalent circular diameter, aspect ratio, intensity). BMI can achieve high sample throughput at required sample volumes below 100 µL. In principle, for samples containing very low particle concentrations, higher volumes up to several mL could be applied in multiple successive application steps to achieve statistically sound results. Owing to liquid removal in the membrane filtration step, the impact of formulation refractive index and interferences by microbubbles and droplets (e.g., silicone oil) are eliminated [47–49]. Accuracy of particle counting can be compromised by the limited field of view of the optical system [47]. Further, the required membrane filtration as part of the sample preparation might pose a risk to the integrity of fragile particles [50]. Recently, BMI has advanced into fluorescence membrane microscopy, which complements BMI by fluorescence imaging options [51].

### Imaging flow cytometry (IFC)

IFC, originally designed as a cytometric tool, is a technique combining conventional flow cytometry with imaging microscopy. Available channels for signal collection and image acquisition comprise brightfield, fluorescence, and side scattering mode [52]. In the field of particle analysis, IFC is intended to allow for the discrimination of different particle types (e.g., proteinaceous, silicone oil) based on the fluorescent labeling of particles [53–55]. Currently marketed instruments are the FlowSight and the ImageStream$^X$ Mk II (Luminex, Seattle, WA). Depending on the instrument set-up, IFC allows for the analysis of particles down to approx. 1 µm in size or even in the submicrometer size regime. From the collected images, a broad selection of parameters (size, shape, intensity, texture, etc.) can be evaluated with the help of user-defined image analysis masks [52, 56]. IFC instruments process sample volumes as low as 20 µL and were reported to offer superior sensitivity for particle detection when compared to currently available flow imaging microscopes. Nevertheless, IFC exhibits limitations in the analysis of samples containing low particle numbers as baseline levels up to $3\times10^6$ particles/mL have been reported in measurements of deionized water with the ImageStream$^X$ instrument [53].

### Oil-immersion flow imaging microscopy (OI-FIM)

OI-FIM is an extension of the flow-imaging microscope series provided as FlowCam Nano by Fluid Imaging Technologies. Compared to other flow-imaging microscopes, it covers a lower particle size range, i.e., from about 0.3 to 10 µm. This is achieved by using an oil-immersion technique with a numerical aperture of 1.4 and a blue light-emitting-diode (LED) as light source [57]. Similar to other flow-imaging microscopes, particle characterization is based on high-resolution images, from which 40 diverse optical parameters can be retrieved for each particle, e.g., several types of diameter, shape, intensity and translucency. Although the current set-up has some limitations, such as light-scattering artefacts and an ill-defined measured volume, the instrument can be used for sizing, morphological characterization and quantification of particles from various sources [58]. The FlowCam Nano provides an important microscopic tool to close the analytical gap in the field of submicron (and low-micron) particle analysis. Currently the lower limit for particle discrimination based on morphological parameters was found to be at approx. 2 µm [58]. A discrimination of even smaller silicone oil droplets and protein aggregates could be achieved by using deep learning tools [59].

### Holographic video microscopy (HVM)

With HVM particles can be analyzed directly in the formulation buffer, without any sample preparation or dilution. Based upon the Lorenz-Mie theory of light scattering the size and the refractive index of particles can be determined [60]. The covered size range spans from 0.5 to 10 µm with particle concentrations from $1x10^3$ up to $1x10^7$ particles/mL [61]. HVM was successfully used to discriminate protein aggregates from silicone oil droplets in the presence of surfactants [62]. Additionally, other particles commonly encountered in drug product development, such as metal particles, degradants of surfactants and air bubbles, can be distinguished with HVM [61].

### Machine learning tools

Many particle analysis techniques such as flow imaging microscopy (FIM), imaging flow cytometry or Raman spectroscopy acquire a large amount of data. In order to increase information extracted from this data, machine learning tools can be used. In general, machine learning is based on algorithms detecting patterns in data, which can then be used to build models to make predictions on unknown data. Several approaches, such as supervised or unsupervised learning, are applicable for drug product development. In-depth explanations of available machine learning models and their relevance for the development of biopharmaceuticals were provided by Kamerzell et al. and Narayanan et al. [63–65].

Machine learning can be used to understand particle formation of biopharmaceuticals in order to adapt drug product manufacturing or give recommendations regarding proper handling thereof. In recent years, the application of machine learning was successfully applied to improve the

characterization of protein therapeutics with regard to particle classification, as well as root-cause analysis for protein aggregation [66, 67].

## Application of particle techniques for characterization of therapeutic protein formulations

### Protein-related particles

When proteins aggregate in solution, porous structures containing solvent are formed [68], which explains why the density of protein aggregates is typically lower than that of the protein monomer [69]. Micrometer-sized aggregates contain 80-93% water, whereas smaller aggregates most likely contain less solvent, as their density approaches the protein's density with decreasing aggregate size [69]. Depending on the method's measurement principle, the resulting size of a protein aggregate can be described by a number of different diameters (Figure 2). Moreover, in solution, protein aggregates are surrounded by a hydration shell. Consequently, techniques analyzing the protein aggregate in solution may provide different size information compared to techniques which analyze the sample after solvent removal. Therefore, when comparing "the size" of protein aggregates between methods, it is key to consider which type of diameter has been acquired and by which particle technique sizing has been performed.

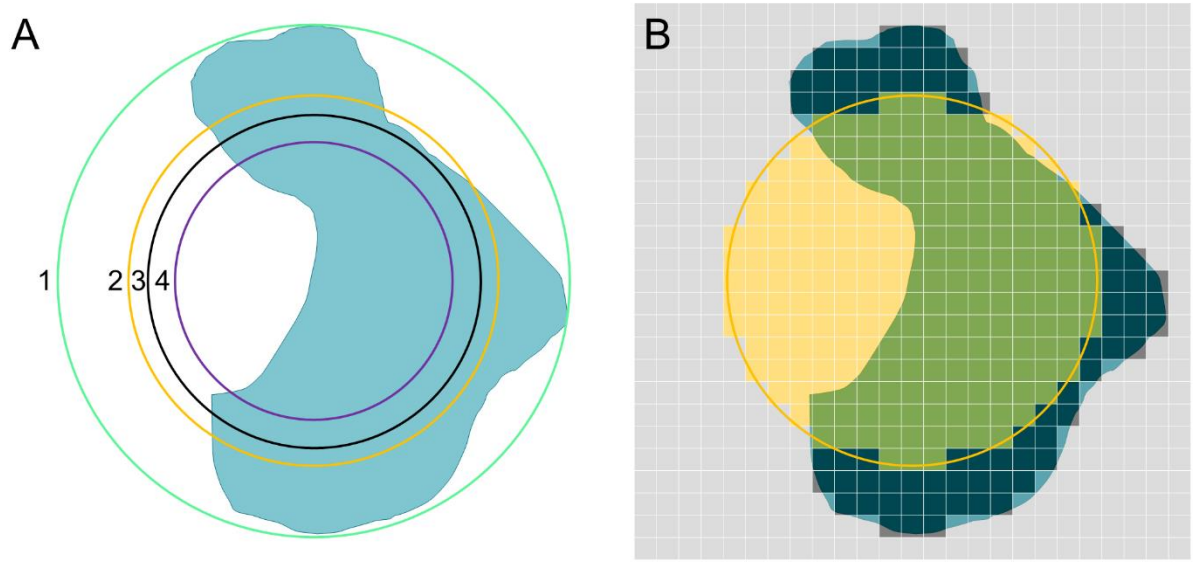


*Figure 2: Illustrated 2D projection of a hypothetical protein aggregate (light blue) in the submicron size range. A) Green ring (1): Feret diameter (e.g., OI-FIM); Orange ring (2): equivalent circular diameter or area based diameter (e.g., OI-FIM); Black ring (3): 2x root mean square distance or 2x radius of gyration (e.g., SAXS, SLS); Purple ring (4): 2x hydrodynamic radius or 2x Stokes radius (e.g., AUC, DLS, NTA), assuming an arbitrary Rg/Rh of 1.2 for elongated fractal structure.[100] B) Grey grid: illustrated pixels from a digital camera; Dark area: pixels covered by the projected protein aggregate; Yellow area: Pixel area of an equivalent circle; Orange ring: equivalent circular diameter or area based diameter.*

In solution, the protein size in terms of hydrodynamic radius (Stokes radius, Rh) can be approximated from size exclusion chromatography (SEC) by comparing the retention times to those of reference

proteins [70–72]. In case of SEC, the lower and upper separation size limit of the protein and its aggregates are restricted by the pore size of the stationary phase. In contrast, the hydrodynamic radius can be obtained more straightforward by using analytical ultracentrifugation (AUC), dynamic light scattering (DLS), and nanoparticle tracking analysis (NTA). Depending on the speed of rotation, AUC can be applied to either small proteins, as well as larger aggregates in case their abundance is high enough for detection.

Because individual particles are analyzed, NTA and resistive pulse sensing (including MRPS and TRPS) can resolve protein particles with heterogeneous size in the submicron-size range and thus provide better particle size distributions compared to ensemble analysis from DLS [73, 74].

Small angle X-ray scattering (SAXS)[75] and, above approx. 10 nm, multi angle light scattering (MALS) provide the size in terms of radius of gyration (Rg). MALS in combination with SEC or field flow fractionation (e.g., AF4) is very powerful to obtain the size of monomers and oligomers after separation [76].

Techniques which can analyze protein particles in the dried state are for instance light microscopy after filtration (including backgrounded membrane imaging, see section on BMI), atomic force microscopy (AFM) [77], as well as (negative staining) electron microscopy (EM) [68, 78]. Moreover, protein particles can be studied in the frozen-hydrated state by electron microscopy (cryo-EM)[68] and in solution (liquid cell EM) [79]. Remarkably, AFM can also measure protein aggregates adsorbed to relevant surfaces such as glass barrels from syringes [80].

From imaging techniques in general, several morphological aspects of (sub)micrometer-sized protein aggregates can be obtained, such as Feret diameter and the frequently used equivalent circular diameter (Figure 2). For porous particles it depends on the measurement principle (e.g. light-based vs. mass-based or electrical-current-based) and/or the analysis settings (e.g., threshold values in imaging techniques) whether the particle size is reported including or excluding the porous parts filled with formulation buffer.

Typically, a particle size distribution is obtained which either describes the mass (per volume) or the number (per volume) of detected protein aggregates across the size range covered by the method. SEC is most routinely used as workhorse method for quantification of the monomer and smaller oligomers. AUC[81–83] and AF4[83, 84] provide similar information but from orthogonal measurement principles. Nevertheless, SEC, AF4, and AUC quantify the mass of each species after separation typically via UV, RI or fluorescence detection. In contrast, DLS provides the size distribution by scattering intensity of the ensemble as a result.

The molecular weight of a protein oligomer is typically a better indicator for the stoichiometry (e.g., dimers, trimers, etc.) than its size. Several methods provide the molecular weight of the protein aggregate such as AUC [85], mass photometry [86], as well as SEC and AF4 via calibration or in combination with MALS detectors [76, 87].

For counting of submicron protein particles, single particle analysis techniques such as NTA, MRPS, TRPS, RMM, OI-FIM are clearly favored over ensemble analysis from, e.g., DLS [88, 73, 74]. A continuous particle size distribution from nanometer- to micrometer-sized protein aggregates, with exponentially decreasing particle concentrations with increasing particle size can very often be observed [58], but is not guaranteed. For example, Filipe et al. also reported a discontinuity of the particle size distributions from NTA, RMM, and MFI [89]. To obtain statistically significant results, the small analyzed volume is typically a challenge when using submicron methods [25–27, 88], whereas the low relative number-based abundance of large protein particles is challenging for methods in the micrometer-size range [90]. Moreover, authors have reported challenges with RMM [25, 44] and NTA [25, 91, 92] regarding their measurement performance for protein samples, including recommendations for best practices.

Importantly, particle concentrations obtained from orthogonal methods will always differ, to a small or large extent. This has been demonstrated and discussed many times, e.g., for LO and FIM [26, 27, 93–96], resistive pulse sensing, RMM and NTA [26, 27], MRPS [88], BMI [47], OI-FIM[58], and has many reasons including measurement principle, properties of the particles and the surrounding solution, and instrument limitations. Differences in outcome do not necessarily mean that one technique is more “right” or “wrong” than the other, but instead can be employed to gain a better insight into the aggregate content of a sample.

In general, methods which provide information additional to size and quantity are very interesting for protein product development or trouble shooting. For example, HVM measures the refractive index of individual subvisible particles (see section on HVM). Microscopes in combination with an Fourier-transform infrared spectroscopy (FTIR) or Raman spectrometer can reveal the chemical composition and therefore are used for forensic applications. FTIR and Raman are complementary spectroscopic techniques for the identification of organic compounds, with the help of spectral libraries for comparison [97]. Also, energy dispersive X-ray (EDX) spectroscopy, which is commonly coupled to a scanning electron microscope (SEM) providing detailed particle morphology, can be applied for particle identification [98]. Knowing the particle composition is of high relevance to understand the source of particles, as well as particle formation and/or aggregation mechanisms. Useful case studies describe optimized isolation and analysis workflows for particle identification based upon the expected particles and microscopic inspection [99].

Different stress conditions cannot only impact the size and counts, but also the morphology of protein aggregates, which can be directly observed by, e.g., microscopic techniques [67, 66], or indirectly for instance by determining Rg/Rh (Figure 2) [100, 101]. Machine learning tools can extract stress signatures from the morphology of protein particle images [66, 67, 102]. Convolutional neural networks (CNNs) alone or in combination with data pooling [67], classifiers such as k-nearest neighbor or support vector machines [66] and statistical analysis [102] can accurately predict the particle origin.

**Excipient-related particles**

In addition to the protein, excipients in therapeutic protein formulations can contain particles and/or form particles due to degradation. Along with the wide application of polysorbates to protect proteins against interfacial stress, water-insoluble free fatty acids (FFAs) have received growing attention as source of particles [103–105]. FFAs are commonly formed during enzymatic ester hydrolysis of polysorbate by trace amounts of residual host cell proteins [106–108], but an oxidative pathway releasing FFAs is also described [109]. Besides FFA-related particles an increase in proteinaceous particles can occur due to the loss of functional polysorbate after hydrolysis [48]. Both, the formation of FFA-related particles and proteinaceous particles will impact the quality of a drug product; specifications for visible or subvisible particles may no longer be met. In addition, FFA-related particles can exhibit a morphology closely resembling proteinaceous particles, thus impeding a straight-forward discrimination of the two particle classes based on imaging techniques. Low-throughput techniques, such as FTIR and Raman microscopy, are frequently applied to allow for the identification of particles resulting from polysorbate degradation [105, 110–113]. Heterogeneous particles composed of protein and polysorbate-related FFA were analyzed by using FTIR microscopy and SEM-EDX [110]. Additionally, both techniques were also used to identify particles from FFAs in complex with glass leachables [114].

Furthermore, Winters et al. described holographic video microscopy as a novel approach for the discrimination of FFA-related particles (oleic acid droplets) from protein particles and silicone oil (SO) droplets in a mixed sample [61]. Nevertheless, the authors also revealed the limitations of the technique when analyzing samples containing particle classes of similar refractive index as in the case of stearic acid particles and protein particles.

Sugars, such as sucrose and trehalose, are another important class of excipients applied to stabilize therapeutic proteins and as tonicity agents [115, 116]. Remarkably, Weinbuch et al. showed that pharmaceutical grade sucrose can contain up to $10^9$ nanoparticles per gram with a particle size ranging between 100 nm and 200 nm [117]. Those sugar-related nanoparticles were found to interfere with the analysis of submicrometer-sized protein aggregates in DLS and NTA, thus posing a challenge for the application of both techniques in protein formulation development. By using SEM-EDX and FTIR, the authors identified the nanoparticles as impurities from the sugar refinement process. In addition to

compromising protein particle analysis, the observed sucrose-related nanoparticle impurities were shown to be capable of destabilizing mAbs [118].

### Primary packaging material-related particles

In the discussion of particles in therapeutic protein formulations, the primary packaging needs to be considered as a relevant source of particulate impurities. For instance, interaction of the formulation with the primary packaging material or mechanical stress can result in the detachment or shedding of various particles from primary packaging [119–121]. Particles originating from primary packaging materials can affect the quality and safety of a therapeutic protein product in a similar way as particles originating from the formulation itself [122–127]. In order to define a strategy for the mitigation of particle levels in protein therapeutics, understanding particle generation related to primary packaging remains a crucial task [119, 120, 124].

A particle species frequently observed and expected in formulations stored in primary packaging systems containing siliconized surfaces (e.g., siliconized vial stoppers, prefilled syringes) are SO droplets [40, 128]. Noteworthy, SO droplets are primarily considered a safety concern when serving as a nucleation site for protein aggregation, or in case of intravitreal application; otherwise SO is deemed less critical [39, 122, 123, 129–133]. Accordingly, analysis of SO droplets often focuses on the discrimination of pure SO droplets from other particle types, particularly protein aggregates (or, in addition, mixed SO-protein aggregates). For analysis by flow imaging microscopy, multiple approaches have been published to differentiate SO droplets and protein aggregates with the help of image-based morphological filters which consider one or multiple morphological features, such as aspect ratio and intensity parameters [35, 37, 124, 128, 134–137]. More recently, FIM-based particle classification has advanced further with the help of machine learning approaches [67, 134, 135]. A random forest approach, a supervised learning algorithm based on morphological parameters, can be used to discriminate silicone oil and non-silicone oil particles in FIM images [134]. Further, image-based filters based solely on silicone oil images obtained by FIM can also be applied to classify SO droplets and non-SO particles with principal component analysis (PCA) [135]. Interestingly, artificial intelligence has lately also been applied as a tool for particle classification in brightfield channel images from IFC [138]. The authors used a CNN and fluorescence staining for verification to differentiate SO droplets, protein adsorbed silicone as well as protein aggregates. Importantly, image-based particle classification still remains challenging in the low micrometer size range because of limitations of the optical resolution of the applied imaging system [58]. Next to data analysis approaches, fluorescent dyes can be applied to identify SO droplets. Examples of the latter include the analysis of BODIPY-labeled SO droplets in IFC or flow cytometers [53, 54, 139]. Furthermore, RMM and HVM represent interesting options for the analysis of SO droplets in the low micrometer and the submicrometer size range. Whereas in RMM, positively buoyant SO droplets can

be discriminated from negatively buoyant particles, such as protein or rubber particles [35, 124, 128, 140], HVM allows for a direct identification of SO droplets via refractive index determination [61, 62]. Chemical identification of SO droplets in aqueous solution can also be performed by Raman microscopy [141]. FTIR microscopy [142], Raman microscopy [143] or FTIR microscopy in combination with SEM-EDX[98] allow the identification of protein and SO in heterogeneous particles.

Other packaging-related particles comprise glass particles originating from glass vials and elastomeric particles from rubber stoppers [99, 120, 125, 126, 128, 137]. Remarkably, glass particles can exhibit comparably large morphological heterogeneity depending on the mechanism of their formation: chips and lamellae resulting from mechanical or chemical stress are of crystalline morphology, whereas silica dissolved from a vial's inner glass surface can form gel-like particles [144].

Approaches to assess glass and rubber particles include visual inspection, light obscuration, optical microscopy, flow imaging microscopy, without necessarily being capable to differentiate glass particles from other types of particles and particle ID techniques [99, 127, 128, 137, 144–147]. During visual inspection, the observation of twinkling effects can give an indication on the presence of crystalline glass particles [127, 144, 145]. Nevertheless, it has been reported that non-glass particles as, e.g., metal particles, can cause similar optical effects, thereby leading to a misinterpretation of particle origin [144, 147]. In the subvisible size range, LO was mainly reported as a tool used in extraction or durability studies testing the emergence of glass or rubber particles in the absence of drug product [128, 145]. For the actual discrimination of glass lamellae or rubber particles from formulation-related particles (e.g., protein particles), optical microscopy and flow imaging microscopy were shown to be useful techniques [127, 128, 137, 144, 145]. These microscopic approaches were reported to allow trained operators to classify particles by morphological appearance down to a minimum particle size of roughly 10 µm [145] or even 5 µm [137]. Nevertheless, according to Akhunzada et al. the identification of glass and rubber particles by flow imaging microscopy combined with the application of image-based morphological filters still remains challenging [137].

For an in-depth analysis of particle origin, particle ID techniques, specifically SEM-EDX and FTIR microscopy, are applied in the pharmaceutical industry [99, 127, 144–146, 148, 149]. In contrast to liquid SO droplets, glass particles and rubber particles are retained on membranes and filters applied during sample preparation for SEM-EDX or FTIR microscopy, allowing for the analysis of the spectral properties and thus chemical composition of the particles. To date, multiple studies have demonstrated the successful identification of glass particles in placebo formulations or actual therapeutic protein products with the help of both techniques [144, 148, 149]. Mixed particles consisting of protein and silicone rubber particles were identified by Raman microscopy and IFC [97]. Raman microscopy can also be applied for the in situ identification of particles as shown for cellulose fibers

and polypropylene particles [141]. For the identification of inorganic compounds such as metals and for an element analysis SEM-EDX can be used [99].

## Application of particle techniques for characterization of particulate biopharmaceutical formulations

### Virus particles

The majority of gene therapy viral vectors is based on adenovirus (AdV), adeno-associated virus (AAV) or lentivirus (LV) [14]. In addition, more than 30 different types of oncolytic viruses have been studied in clinical trials [150]. Here, we summarize key characteristics of selected virus particles of pharmaceutical interest used as viral vectors or oncolytic viruses, and give an overview on analytical techniques for characterization of these virus particles by size, shape, content and concentration. It should be noted that methods described in previous chapters can also be used to monitor subvisible and visible particles potentially present in viral preparations, e.g., residual process-related protein particles or particles originating from the packaging material (Figure 3).

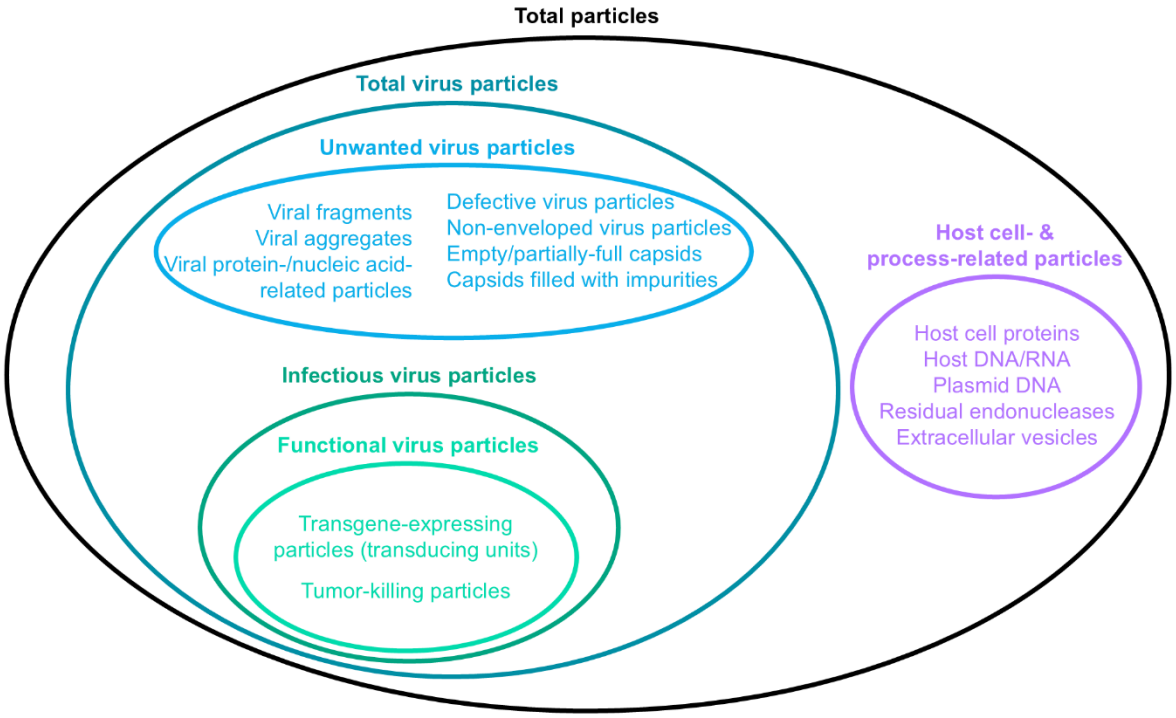


*Figure 3: Overview of different particle types found in viral formulations. Viral formulations may contain host cell- and process-related particles (purple) as well as virus particles (dark blue). Total virus particles may be unwanted virus particles (light blue) such as viral fragments/aggregates or wanted infectious virus particles (dark green). Functional virus particles, i.e., particles that reach the desired effect (light green), are a subgroup of infectious virus particles.*

Commonly applied virus particles are in a size range of 20 to 360 nm and mostly spherical or icosahedral in their morphology (Table 2). The variety of used virus types is high, including enveloped and non-enveloped, RNA and DNA viruses with genome sizes from 4.7 to 280 kb. Product-related impurities such as viral aggregates (larger in size than target virus particles) or fragments (smaller in size) and free viral proteins or nucleic acids exist in preparations of all virus types. Free viral proteins, sometimes associated with DNA/RNA, may precipitate and form particulate impurities in the viral vector preparation. Empty particles (similar size as target virus particles) are a frequent impurity in AAV, AdV and Parvovirus H1-PV products [18, 20, 151]. LV and measles virus (MeV) preparations may be affected by particles with disrupted or without envelope [18, 152]. Most process-related impurities, e.g., host cell proteins and nucleic acids, residual endonucleases, adventitious agents, extracellular vesicles, etc., appear in all virus preparations [18, 152, 153] and may form additional particles. Consequently, particle characterization of viral formulations is challenging, because of their heterogeneity and the large concentration range over several orders of magnitude for the different particle types [18, 154].

*Table 2: Characteristics of selected viruses used in oncolytic and viral vector applications*

| **Virus type** | **AAV** | **Parvovirus H-1PV** | **Poliovirus** | **Reovirus** | **AdV** | **γRV** | **LV** | **VSV** | **HSV** | **SeV** | **MeV** | **VACV** |
|---|---|---|---|---|---|---|---|---|---|---|---|---|
| **Size (nm)** | 20-25 | ~26 | ~30 | 85 | 70-100 | 80-100 | 80-120 | 185 x 75 | 155-240 | 260 | 100-300 | 360 x 270 x 250 |
| **Morphology** | Icosahedral | Icosahedral | Icosahedral | Icosahedral | Icosahedral | Spherical | Spherical | Bullet-shaped | Spherical | Spherical | Pleo-morphic (roundish to rod-like) | Brick-shaped |
| **Envelope** | No | No | No | No | No | Yes | Yes | Yes | Yes | Yes | Yes | Yes |
| **Genome type and size (kb)** | ssDNA ~4.7 | ssDNA 5 | ssRNA 7.2-8.4 | dsRNA 22-27 | dsDNA 26-45 | ssRNA 7-12 | ssRNA 7-12 | ssRNA ~11 | dsDNA 120-200 | ssRNA ~15 | ssRNA 16-20 | dsDNA 130-280 |
| **Main application** | GT (mainly *in vivo*) | OV | OV | OV | GT, OV, VV | GT | GT (mainly *ex vivo*) | OV | OV | VV | OV | OV |
| **Product-related impurities** | Viral aggregates; viral fragments; non-particle associated viral proteins/ nucleic acid<br>Defective/inactive particles; non-enveloped particles (LV); particles with disrupted envelope (MeV); empty particles (AdV, AAV, H-1PV); partially full capsids (AAV); capsids filled with nucleic acid impurities (AAV)<br>Wild-type AdV, helper AdV; wild-type AAV; replication-competent provirus (mainly first- and second-generation LV) | | | | | | | | | | | |
| **Process-related impurities** | Host cell protein/DNA/RNA (may aggregate to particles)<br>Plasmid DNA (dependent on production process)<br>Residual endonucleases, adventitious agents (e.g., cell dissociation enzyme), residual cesium (for AdV, AAV)<br>Mycoplasma, bioburden, endotoxin<br>Extracellular vesicles | | | | | | | | | | | |
| **Key references** | 14, 19, 20, 251 | 18 | 252, 253 | 18 | 14, 18, 151 | 14, 19 | 14, 19, 152 | 252, 254, 255 | 18 | 256 | 18, 257 | 18 |

**Abbreviations: AAV: adeno-associated virus; AdV: adenovirus; GT: gene therapy; HIV-1: human immunodeficiency virus type 1; HSV: herpes simplex virus; kb: kilo base; LV: lentivirus; MeV: measles virus; MLV: murine leukemia virus; OV: oncolytic virus; SeV: Sendaivirus; VACV: vaccinia virus; VSV: vesicular stomatitis virus; VV: vaccination vector; γRV: gammaretrovirus**

Table 3 gives an overview of analytical techniques that are used to characterize virus particles by their size, shape, content (cargo load, e.g., empty vs. full capsids) and concentration; main advantages, limitations and key applications are also summarized. Virus particle concentrations can be measured by different methods leading to distinct particle titers. Here, we distinguish concentrations of total virus particles, infectious and functional virus particles (Figure 3). Most methods determine and characterize the total virus particle concentration, e.g., dye-based binding assay (DyeBA), enzyme-linked immunosorbent assay (ELISA), field-flow fractionation-multi-angle light scattering (FFF-MALS), NTA, polymerase chain reaction (PCR) methods, product-enhanced reverse transcriptase (PERT) assay, SEC and TRPS. Different numbers for the total virus particle concentration are achieved depending on the applied methods due to differences in the measuring principles. For example, the total virus particle concentration of an LV sample was higher when measured by quantitative reverse transcription PCR (RT-qPCR) than by TRPS, presumably because RT-qPCR quantifies all viral RNA genomes independent from particle size whereas TRPS requires particles of the appropriate size [155]. Infectivity assays, such as 50% tissue culture infective dose ($TCID_{50}$) and plaque assays, selectively measure the concentration of infectious virus. The functional titer can be determined in potency assays by measuring the desired effect, i.e., transgene expression or tumor killing capacity. Noteworthy, current methods cannot assess functional or infectious titer and total virus particle concentrations simultaneously [154]. Obviously, functional or infectious titers are mostly lower than total virus titers, and ratios of total to infectious particles can vary even for different preparations of the same virus. For example, the ratios span from 4 to over 200 for AdV, depending on batches and analytical methods used [151, 155, 156]. For vesicular stomatitis virus (VSV), in contrast, a value of about one was reported when comparing infectious titer from plaque assay with total particle concentration from TRPS [156], whereas for LVs values are in the $10^3$ order of magnitude for the ratio of total to functional particles [153]. Due to the divergence of total virus particle numbers, infectious and functional titers, a full characterization of virus particle concentration requires multiple and complementary methods.

Some of the used analytical techniques are restricted to certain virus types, e.g., PERT assay uses the viral reverse transcriptase activity to estimate particle concentration of LV or γRV [153, 155], whereas others can be applied for all viruses, e.g., transmission electron microscopy (TEM) for investigating morphology of single virus particles [155]. TEM is also the reference method to determine the content ratio (i.e., fraction of capsids with a complete genome) of AAV, while sedimentation-velocity analytical ultracentrifugation (SV-AUC) is the standard method to quantify partially-full AAV capsids and quantitative PCR (qPCR) to titer AAV genomes [20]. The recently developed multiwavelength SV-AUC can assess full, empty, partially-full AAV and aggregates [157].

Beside these well-established methods, new techniques are emerging for virus particle characterization, such as ILM ("Videodrop"), flow virometry, mass photometry and native mass spectrometry (MS). Videodrop is a nanoparticle counter based on transmission brightfield microscopy that was used to analyze LV and AdV samples [158]. Flow virometry enables the characterization of virus particles down to approx. 100 nm diameter by fluorescent labeling of virus particles with antibodies, RNA/DNA or envelope dyes. Alternatively, recent technical advancements of standard flow cytometers also allow measurements of virus particles without additional staining [159]. The ultrasensitive nano-flow cytometer (nFCM) expands the detection range to 27 nm for virus particles by reducing background signals [151]. Flow virometry has been used to characterize and quantify a range of different viruses including vaccinia virus (VACV), HSV, human immunodeficiency virus (HIV), reovirus and AdV [151, 159]. Mass photometry was used to obtain the count-based particle distribution of empty and genome-filled AAV [160]; its full potential and limitations are still under investigation. Native MS is another emerging analytical technology in structural virology with great potential despite the difficulties due to the high mass (into megadalton range), relatively low number of charges and the inherent microheterogeneity of the virus particles [161, 162]. Improved mass analysis of intact viruses or virus-like particles was achieved by charge detection-mass spectrometry (CD-MS), ion mobility spectrometry (IMS)-MS, gas-phase electrophoretic mobility molecular analysis (GEMMA) and nanoelectromechanical system-mass spectrometry (NEMS-MS) allowing for example analysis of single virus particles [163]. Orbitrap-based single-particle CD-MS was successfully applied to differentiate empty and loaded AAV8 particles [164]. The use of MS for virus particle characterization will certainly expand beyond current research institutions once appropriate MS instruments will be commercially available.

*Table 3: Overview of analytical methods for characterization of particulate biopharmaceutical formulations, i.e., virus particles, vaccines, virus-like particles (VLP), lipid nanoparticles (LNP), and cell-based medicinal products (CBMP).*

| Method | Target information | Advantages | Drawbacks | Application examples | Key references |
|---|---|---|---|---|---|
| AEX | Particle content[a] | High throughput and reproducibility; read-out via OD, FS or light scattering | Poor resolution of empty vs. full capsids; method development required for each serotype | AAV | [20, 258] |
| AUC | Particle content | Differentiation of empty, partially-full, full particles and aggregates; highly repeatable | Large sample volume at high concentration needed; low throughput; purified samples required | AAV | [20, 157] |
| | | | | Hep E VLP | [182] |
| | | | | siRNA LNP | [199] |
| Coulter counter | Particle size<br>Particle concentration by counts | Simple and fast; direct determination of size | No discrimination of particle classes possible | CBMP | [208, 209] |
| Cryo-EM | Particle size<br>Particle morphology/content | Minimum sample preparation; high optical resolution; very limited modification of virus particles; analysis of impurities | Expensive; low throughput; difficult to get statistically relevant particle information | AAV | [20, 259] |
| | | | | Influenza VLP | [185] |
| DLS | Particle size | Non-destructive; fast; information on polydispersity, PSD, aggregation; might be combined with SLS | Unreliable results for more polydisperse samples; poor precision | LV, AAV | [260, 261, 20, 262] |
| | | | | Duck malaria-HepB VLP | [187] |
| | | | | siRNA LNP | [203] |
| DyeBA | Nucleic acid concentration (by dye) → particle concentration | Simple and fast; alternative to PCR methods, not genome-sequence dependent | Requires removal of free nucleic acids; less sensitive than PCR; accuracy and robustness to be determined | AAV | [20] |
| ELISA | Capsid protein concentration → particle concentration (capsid titer) | High specificity, robustness | Measured viral protein might not be part of virus particle (particle purity required); time- and labor-intensive | H-1PV, AAV, LV | [18, 19, 155, 20] |
| FFF-MALS | Particle size<br>Amount → particle concentration | Includes fast and gentle sample separation; information on PSD and aggregation | Laborious set-up and optimization of separation conditions | AdV, LV | [155, 263, 264] |
| | | | | Attenuated influenza virus | [165]<br>[167] |
| | | | | Inactivated influenza virus | [180] |
| | | | | HBsAg VLP | [200] |
| | | | | siRNA LNP | |
| Flow Cytometry | Particle characterization | Versatile (cell viability, identity and functionality); standard technique in cell biology | Time consuming sample preparation; different staining dyes required | CBMP | [216, 223] |
| Flow-Imaging microscopy | Particle size<br>Particle concentration by counts<br>Particle characterization | Visualization of particles; discrimination of particle classes; combinable with machine learning tools | Laborious set-up | CBMP | [231, 221, 220] |

| Method | Target information | Advantages | Drawbacks | Application examples | Key references |
|---|---|---|---|---|---|
| Flow virometry | Particle size<br>Particle content<br>Particle concentration by counts | Single-particle method; high throughput; low sample volume; characterization of envelope conformation | Detection limit at 25 – 100 nm; measurement in the lower size range might be inaccurate | AdV, HSV, HIV, VACV, reovirus, AAV | [151, 159, 158, 20] |
| | | | | Influenza virus | [169] [189] |
| | | | | HIV-1 VLP | |
| Fluorescence microscopy | Particle characterization | Simple, cell viability by staining | Low throughput | CBMP | [217] |
| FTIR spectroscopy | Particle characterization | Mechanistic information (membrane phase transition, ice melting) | Low-throughput; complex data evaluation | CBMP | [239] |
| ILM ("Videodrop") | Particle size<br>Particle concentration by counts | Fast for moderate number of samples; easy to use; low sample volume | For nanoparticles > 70 nm; difficult for low-concentration samples with impurities; narrow concentration range: $10^8$-$7x10^9$ particles/ml | AdV, LV | [158] |
| Light microscopy | Particle concentration by counts<br>Particle size<br>Particle characterization | Simple; automated and semi-automated instruments available; cell viability by staining | Low throughput (manual counting) | CBMP | [218, 211] |
| Mass photometry | Particle content | Fast; small sample volume | Accuracy, precision, robustness to be determined | AAV | [20, 160] |
| Native MS | Particle mass and composition<br>Particle content<br>Particle concentration by counts | Selective analysis of single virus particles; analysis of particle interactions with other molecules | Used MS instruments still in research state; high expertise needed; highly demanding data analysis | AAV | [161, 162, 164] |
| NTA | Particle size<br>Particle concentration by counts | Fast; high-resolution PSD; label-free and fluorescence label possible | Limited concentration range: $10^7$ -$10^9$ particles/ml; large sample volume; limited accuracy | AdV, LV, HSV | [158, 155, 265] |
| | | | | Inactivated rabies virus | [168] [177] |
| | | | | HIV 1 gag VLP | |
| OD 260/280 nm | Particle content<br>Protein/nucleic acid absorbance → particle concentration by specific extinction coefficient | Fast, automatable | Limited to concentrated samples free from residual nucleic acids and proteins; prone to interferences; small linear range; low precision | AdV, AAV | [18, 19, 20] |
| PERT assay | Reverse transcriptase activity → particle concentration by known activity per virion | More stringent than capsid titer | Works only for *retroviridae* (functional reverse transcriptase required) | RV, LV | [155, 153, 266] |
| Plaque assay | Number of plaques → infectious titer | Cell-based infectivity assay | Virus replication in culture needed; time- and labor-intensive | HSV, VACV, AdV, H-1PV, VSV | [18, 19, 155, 265, 156] |

| Method | Target information | Advantages | Drawbacks | Application examples | Key references |
|---|---|---|---|---|---|
| qPCR, qRT-PCR, ddPCR | Viral genome concentration → particle concentration (genome titer) | Specific, fast; ddPCR more accurate than qPCR | Requires removal of free viral nucleic acids; requires standard (qPCR, qRT-PCR); ddPCR less mature than qPCR | VACV, AdV, MeV, H-1PV, AAV, γRV, LV, AdV | [18, 19, 153, 20, 158] |
| Raman microscopy | Particle characterization | Versatile (cell viability, identity); mechanistic information (membrane interactions); in-situ analysis | Complex data evaluation; | CBMP | [233, 228] |
| SEC | Particle content<br>Amount → particle concentration | Fast; commonly used for information on aggregation (AAV); read-out via FS, MALS or OD | Non-specific interactions possible; decomposition of large aggregates possible | AAV, LV<br>Live attenuated Influenza virus<br>HIV-VLP<br>siRNA LNP | [20, 266, 258]<br>[165]<br>[177]<br>[198] |
| Target tumor cell killing assay | Amount of tumor cell killing → functional titer | Cell-based potency assay | Time- and labor-intensive | HSV, VACV, AdV, MeV, H-1PV | [18] |
| $TCID_{50}$ assay | Number of infected wells (dilution-dependent) → infectious titer | Cell-based infectivity assay | Time- and labor-intensive | Reovirus, HSV, MeV, VSV, AAV, AdV | [18, 255, 19] |
| TEM | Particle size<br>Particle morphology/content | Distinguishes well full, empty, partially-full capsids; direct imaging of sample; analysis of aggregates | Difficult to get statistically relevant particle information; challenging image analysis; low throughput | AdV, LV, AAV, RV, HSV, VSV, SeV, H-1PV<br>Live attenuated influenza<br>Hepatitis E VLP<br>siRNA LNP | [158, 260, 20, 267, 265, 156, 256, 18]<br>[165]<br>[182]<br>[199] |
| Transduction assay | Amount of transgene expression → functional titer | Cell-based potency assay; read-out with flow cytometry, ELISA, PCR or similar | Time- and labor-intensive | γRV, LV, AAV | [19, 153] |
| TRPS | Particle size<br>Particle concentration by counts<br>Particle charge (zeta potential) | Concentration range: $10^5$-$10^{11}$ particles/ml; accurate; nanopore size range: 40 nm – 11.3 µm | Large particulate impurities block membranes | LV, HSV, VSV | [158, 266, 156] |

Abbreviations: AEX: anion-exchange chromatography; AUC: analytical ultracentrifugation; Cryo-EM: cryogenic electron microscopy; ddPCR: digital droplet polymerase chain reaction; DLS: dynamic light scattering; DyeBA: dye-based binding assay; ELISA: enzyme-linked immunosorbent assay; FFF-MALS: Field-flow fractionation-multi-angle light scattering; FS: fluorescence spectroscopy; ILM: Interferometric light microscopy; MS: mass spectrometry; NTA: nanoparticle tracking analysis; OD: optical density; PERT: product-enhanced reverse transcriptase; PSD: particle size distribution; qPCR: quantitative polymerase chain reaction; qRT-PCR: quantitative reverse transcription polymerase chain reaction; SLS: static light scattering; $TCID_{50}$: 50% tissue culture infective dose; TEM: transmission electron microscopy; TRPS: tunable resistive pulse sensing

[a] Particle content means the particle cargo load, e.g., empty vs. full capsids.

### Live attenuated and inactivated viruses as vaccine antigens

Particle analysis to assess product quality is less frequently used for inactivated and live attenuated viral vaccines, as compared to many other biopharmaceuticals (Table 3). Although particle size can have an impact on the immunogenicity, changes in particle composition play a minor role in the (desired) immunogenicity of these products. However, a distinction must be made between live attenuated vaccines and inactivated viral vaccines.

For live attenuated vaccines the viral titer (= all infectious virus particles) is crucial. The number of infectious particles determines the immunogenicity to a large extent, because in many cases attenuated strains replicate after administration. To minimize risks and demonstrate product consistency, the presence of viral aggregates, non-infectious particles or viral fragments should be controlled as unwanted impurity, because it may affect potency, safety and product yield. Sizing and counting methods are suitable to demonstrate batch consistency and quality. This was shown for attenuated influenza vaccine using FFF-MALS, SEC-MALS and TEM for sizing/counting of particles, as well as methods for infectious particles, such as RT-qPCR, fluorescent focus assay and $TCID_{50}$ [165].

For inactivated viral vaccines the presence and formation of aggregates as well as viral fragments is even more critical. Antigen will not be produced in vivo, as with most attenuated vaccines, but all antigen is present in the administered dose. Aggregation or fragmentation should be limited as they may result in inconsistent efficacy.

Electron microscopic techniques have been used to size inactivated SARS-CoV-2 vaccine as a function of different downstream processing steps [166]. Moreover, size based detection of particles by light scattering techniques is mainly used to measure particle size, and sometimes also the number of viral particles. A comparative study of classical quantification methods (infectious particle assays, PCR) and FFF-MALS done with influenza virus shows that FFF-MALS is not only suitable for virus quantification but also provides insight in the presence of aggregates [167]. In addition the assay can be used on the vaccine, i.e., the inactivated virus. However, particle concentration is not a priori potency indicating (see also section on virus particles). Proper process control during downstream processing/vaccine production to ensure consistent removal of unwanted species next to continuous stability programs should guarantee the absence of aggregates or fragments. If this is the case, particle counting may well correlate with antigenicity, as was shown for highly purified rabies vaccine [168]. NTA and ELISA had correlation coefficients of 0.9 or higher. With influenza virus a similar excellent correlation was demonstrated between direct particle counting techniques (TEM and virometry) and indirect methods like ion exchange chromatography and $TCID_{50}$ virus titration [169]. This latter work was performed with live virus, but in principle direct particle counting techniques should also work with inactivated whole virus. Although product release requires functional assays (immunogenicity, potency indicating

antigenicity), these examples demonstrate that particle counting provides extremely valuable supportive information to demonstrate batch consistency, to validate manufacturing steps, for stability assessment, etc.

Measuring the size of inactivated virus in the drug product is often complicated because vaccines contain low concentrations of antigen with doses in the microgram range. In addition, if particulate adjuvants are present (e.g., aluminum salts, oil-in-water emulsions), sizing and counting of the virus particle itself becomes virtually impossible. The adjuvant particles and/or adsorption of the virus particles to the adjuvant prevent reliable size determination of the virus particles.

Thus, since sensitive and reliable sizing [170] and particle quantification techniques [171] for viruses are available, it makes sense to use them routinely in viral vaccine development and QC.

### Virus-like particles (VLP)

Since the introduction of recombinant Hepatitis B surface antigen (HBsAg), which assembles in VLP, in the 1980s, other VLP based vaccines have been marketed. These include influenza [172] and HPV virosomes [173]. Influenza virosomes are also used as an adjuvant or delivery system for non-influenza antigens, such as inactivated hepatitis A virus adsorbed to influenza virosomes [174].

The particulate nature of VLP determines to a considerable extent their immunogenicity. In general, particles with the size of viruses or bacteria (i.e., 20 nm to low micrometer size range) are suitable for immune recognition and activation, with an optimum for smaller nanoparticles (e.g., 50 nm) [175]. From a pharmaceutical point of view VLP should ideally be monodisperse and stable. Particle characterization is therefore important (Table 3).

Size determination by DLS is often used routinely, because it is simple and does not require a lot of material. DLS is a common method to follow VLP formation in refolding and assembly procedures [176] and to assess physical stability. However, in cases where the sample is less monodisperse and/or may contain species of different size such as for partially purified in-process samples, the interpretation of DLS data becomes less straightforward. Therefore, it is recommended to include additional techniques for size analysis of VLP. These methods can be either performed on the sample as it is, like electron microscopy or NTA. In complex samples, containing VLP, VLP fragments (monomeric subunits) and/or VLP aggregates of different size, separation prior to detection can provide more relevant data. The latter approach includes SEC [177, 178] or AF4 [179, 180], both often with MALS detection, and SV-AUC [181, 182].

In the product development phase, particle counting and size measurements are sometimes used as in-process controls to assess product yield for different purification steps [183]. Also, in (early) product development electron microscopic techniques are often used to determine particle size and structure [184–186] in combination with DLS [187] for sizing in the liquid state. Hosseini et al. used DLS, TEM

and SEC to study Hepatitis B surface antigen yield in critical downstream process unit operations [178]. The 25-kD recombinant HBsAg lipoprotein self-assembles into 22-nm VLPs. VLP formation occurs during downstream processing, but unintentional aggregation is a risk, and the formation of VLPs and aggregates in the different unit operations could be mapped. Chen et al used DLS, TEM and AF4-MALS to study salt-induced aggregation of HBsAg and the effect on the antigenicity [180]. Using AF4-MALS three particle populations could be detected and quantified: monomeric particles of 23 nm, oligomers of these particles and polymeric aggregates. The oligomeric fraction was not baseline separated from the monomeric peak but contained monomers, dimers as well as trimers, as observed by TEM. Zhang et al used TEM, DLS, SEC and AUC for particle characterization in addition to other characterization methods, including MS, IEF, SDS-PAGE, CD, UV, DSC, antigenicity and in vivo immunogenicity, to fully characterize a licensed hepatitis-E VLP vaccine [182].

VLP have been used as model analytes to demonstrate, develop and improve sizing and particle counting methods [186, 188–191]. Model bacteriophage VLP with and without two conjugated peptides were used to demonstrate the use two types of field-flow fractionation: AF4 and the better performing cyclical electrical field-flow fractionation (CyEIFF) [190] using MALS detection but also TEM of fractions collected from CyEIFF analysis. For SEC it is possible to increase throughput by interlaced injection, i.e., inject the next sample immediately after the monomeric VLP peak as demonstrated with HPV VLP [191]. Another way to increase throughput is a tiered approach, using a high throughput method (DLS) for screening followed by low throughput methods (AF4) to analyze a selection of relevant samples, as was demonstrated in a formulation optimization study for polyomavirus VLP [192].

SEC-MALS/UV and NTA were assessed for suitability for rapid, automated quantification of HIV-1 gag VLP [177]. MALS detection allowed direct particle quantification without the necessity for calibration curves. Particle concentrations determined by SEC were systematically 1 log lower as compared to NTA measurements, possibly caused by differences in detectable size range and sensitivity. Other approaches include the use of sizing techniques such as NTA, flow virometry, (cryo-)TEM and super-resolution fluorescence microscopy to characterize HIV-1 VLP [189].

### Lipid nanoparticles (LNP)

Particle size of LNP is a critical product attribute, because particle size can affect potency and stability as reported by several groups. Particles in the size range of 40 to 80 nm were considerably more potent than smaller or larger LNP containing si-RNA [193]. Furthermore, the size of LNP may affect targeting to specific organs and the silencing activity of si-RNA, because of differences in adsorption of proteins in the circulation [194]. Also, the size may indicate whether LNP contain active material. This was demonstrated with a SARS-CoV-2 mRNA vaccine, where the mRNA containing LNP were almost 90 nm in hydrodynamic diameter, whereas empty LNP were 55 nm [195]. In all these examples DLS was used to

measure particle size. Given the importance of size, it would make sense to more extensively characterize the particle size of LNPs with orthogonal and complementary methods (Table 3).

DLS in combination with zetapotential measurements has been used in a factorial study design to determine the effect of process parameters and composition on particle size for LNP manufacturing with the emulsion-solvent evaporation technique [196]. For the detection of larger microparticles laser diffractometry was applied. Other characterization techniques included SEM and AFM.

Like for other nanoparticles (cryo-)EM, AFM and DLS allow sizing of LNP in the ensemble of the formulation. In addition, techniques in which the particles are separated first and then analyzed, e.g., AF4 [197], SEC [198], AUC [199] are applied. SV-AUC was used to measure differences in mRNA loading by applying density matching with $D_2O$ [199]. Apart from density variations, particle size and molar mass could also be determined with SV-AUC.

It appears that most sizing techniques for nanoparticles are suitable for LNP analysis. However, care should be taken to avoid "in-analysis" deterioration, because LNP are rather fragile. For instance, although AF4 is thought to cause low stress on the analyte, the focusing step at the start of the procedure may result in aggregation. Mildner et al. optimized the loading and focusing procedures in order to analyze LNP, to finally conduct batch consistency testing, formulation screening and stability testing [200].

Physical stability of LNP is often assessed by DLS, e.g., in stability studies and optimization of (frozen) liquid and lyophilized formulations [201–203].

### Cell-based medicinal products (CBMP)

The main types of current CBMP are cell-based (or *ex vivo*) gene therapy medicines (e.g., chimeric antigen receptor (CAR-)T cells) and somatic cell therapy medicines (e.g., mesenchymal stem cells). Engineered with an artificial T cell receptor CAR-T cells can be designed to specifically target tumor cells [204]. CBMP can be either stored in liquid state (at room temperature or refrigerated), enabling a shelf-life of several hours, or cryopreserved at temperatures below -120 °C for long-term storage up to years (depending on the product) [13]. Methods to determine total cell concentration and viability, as well as flow cytometry for cell identification are commonly used for cell characterization (Table 3). The use of additional particle characterization techniques is not yet common practice. Nevertheless, because of the particulate nature of cells, which are living microparticles, particle analysis may be beneficial in formulation development, manufacturing and quality control of CBMP, as discussed below.

Although cell size is a relatively basic parameter, it can be used as an indicator of cell viability, as dead and apoptotic cells show swelling and shrinking, respectively [205, 206]. Furthermore, changes in cell size

upon exposure to non-isotonic conditions can be used to determine physical parameters, such as osmotically inactive cell volume, water permeability and cryoprotectant permeability. These parameters are critical for the development of cell-specific cryopreservation protocols, including the choice of cryoprotective agents, their addition process as well as an optimal freezing procedure [207]. Established techniques for cell sizing are the Coulter counter [208–210] technique and light microscopy [211–214].

Cell counting is routinely performed in cell culture to monitor cell proliferation and to select reasonable passaging time points. Therefore, viable cells are manually counted in a counting chamber called hemocytometer under a light microscope [215–217]. In order to differentiate between viable and dead cells, the dye Trypan blue can be used, which selectively permeates dead but not live cells. Trypan blue is also used with semi-automated and automated cell counting instruments, where the instrument's software automatically counts viable cells based on image analysis [218, 219].

Another approach for cell counting are FIM techniques. Based on the obtained images from each cell, morphological filters can be developed to determine both total cell concentration and cell viability [220, 221]. The Coulter counter can also be used for cell counting, although a suitable size range has to be defined to minimize contributions of cell debris and aggregates to the overall count [208].

Finally, the characterization of CBMP includes aspects such as cell viability, identity and purity. In general, cell samples can contain viable, apoptotic, dead cells or debris. In addition to Trypan blue, some other dyes are able to stain apoptotic or dead cells, which are subsequently analyzed with fluorescence microscopy [217, 222] or flow cytometry [216, 223]. Raman microscopy is another technique to discriminate viable from dead or apoptotic cells [224]. Furthermore, Grabarek et al. developed a FIM-based method using a CNN to discriminate between viable cells, dead cells and cell debris [221].

CBMP are commonly derived from human material, which consists of various cell types. Therefore, the identification of cells is highly relevant. The classical approach to identify cells is by labeling cell surface markers with fluorescent-dye conjugated antibodies followed by flow cytometry analysis [215–217, 223, 225]. In recent years, several label-free Raman spectroscopy approaches were developed for the phenotyping of immune cells. A line scan Raman method can be used to discriminate between immune cells [226] as well as a combination of single point Raman spectra and digital holographic microscopy [227]. Recently, Akagi et al. developed a Raman spectroscopy set-up based on two rotating Galvano mirrors, which enable the fast acquisition of spectra from a circular cell area [228]. In addition to cell identification, Raman spectroscopy and variations thereof can also be used to determine the activation state of T cells [226, 228, 229].

For differentiation of cells and other particulate components in the sample, FIM is particularly suited, owing to the high-resolution images. Morphological filters can be developed in the instrument's software to differentiate between cells [220, 221], cell debris [221, 230], and process-related impurities such as SO droplets, glass and rubber particles [230]. Furthermore, machine learning tools can improve the discrimination between cells, debris, aggregates and magnetic beads, and potentially other particulate impurities, in FIM images in comparison to classical FIM analysis approaches [221, 231]. Traditional counting approaches can serve for the quantification of residual magnetic beads: After several purification steps the magnetic beads are counted within a chamber under a light microscope similar to cell counting via a hemocytometer [232]. Another approach to quantify residual magnetic beads is to first label them and then apply flow cytometry combined with Trucount® tubes [216].

Raman spectroscopy has been proposed as an in-line control during CBMP manufacturing. By applying multivariate and univariate data analysis of the acquired spectra, nutrient consumption as well as cell concentration and viability can be monitored to ensure optimal cell expansion [233]. Additionally, machine learning can be utilized to understand and predict the impact of the manufacturing processes, including mixing or centrifugation on the cell quality by developing artificial neural networks (ANN) [234]. Raman spectroscopy has also been used for studying cell membrane interactions with cryoprotectants, such as sucrose and trehalose [235], and monitoring intracellular ice formation during freezing [236–238]. Furthermore, FTIR spectroscopy is suited to determine cell membrane phase transitions or ice nucleation and melting [239].

After thawing of CBMP, cell viability and recovery should be verified. For this purpose the already mentioned techniques need to be applied, such as fluorescence microscopy [240], Trypan blue exclusion assays [219, 240] and flow cytometry [241]. Additionally, the functionality of cells should be examined post-thaw, which can be performed by flow cytometry assays based on the labeling of pro-inflammatory cytokines or target and effector cells [242, 243]. Moreover, FIM techniques may be used for the detection of cell aggregates occurring post-thaw [221,244].

### Other biopharmaceutical microparticulate formulations

Other biopharmaceutical microparticulate formulations are, e.g., antibody crystals [245, 246] and depot formulations containing proteins or peptides [247, 248]. Characterization of antibody crystals as well as depot formulations is commonly performed with techniques suitable for the required size range as has been shown by several groups [245–248]. In-depth discussion of biopharmaceutical microparticulate formulations is beyond the scope of this review and can be found in the literature [249].

## Conclusions

Numerous particle analysis techniques are available for the characterization of biopharmaceuticals. The selection of suitable particle techniques is dependent on the product class and the scope of analysis, such as impurity versus active pharmaceutical ingredient or drug delivery system itself.

Whereas ten years ago, particle analysis in biotherapeutic formulations was focused on "unwanted" particles (protein aggregates, impurities, primary packaging related particles) [31], today's particle analysis also covers "wanted" particles (e.g., CBMP, virus particles, VLP, LNP and vaccines). As the available techniques have different benefits and drawbacks, the need to understand the underlying measurement principle remains crucial to select the combination of relevant techniques.

New emerging products such as CBMP and virus particles also require a sharp differentiation and identification of particles. Up to now, the applied analytical particle characterization toolbox for CBMP is limited to a handful of techniques, most of which originate from classical cell culture. As CBMP need to fulfill similar safety requirements as classical biotherapeutics, further analytical developments are required.

Although recent techniques have been developed to close the "submicron particle gap" [250], in particular relevant for protein therapeutics, there are still only few techniques available for this size range, all with specific drawbacks and so far mainly used for characterization. The advance of complex nanoparticulate formulations, such as LNP, VLP, and virus particles, pose new analytical challenges. Furthermore, the analysis of heterogeneous particles in terms of size, composition, origin and function remains challenging with only few techniques being available to identify particles.

Machine learning tools are valuable for the differentiation of various particle classes, as well as they improve the data evaluation for information rich particle techniques. Machine learning is emerging for several analytical purposes, but its full potential is not yet utilized in particle analysis for biopharmaceuticals.

As the complexity of products increases an appropriate combination of techniques should be applied for particle analysis. Such combination of methods is required to cover all aspects of sizing, quantification and characterization over a wide size range from nanometers to micrometers. Orthogonal methods are required to confirm results and gain a good understanding of particle properties because the measurement outcome is depending on the used technique. Last but not least, it is of high relevance to select appropriate techniques regarding the intended purpose. A trouble-shooting analysis of a protein drug product development has different analytical requirements than characterization of virus like particles. Critical quality attributes must be defined for each product class to enable the development of suitable analytical techniques to guarantee a safe drug product.

In conclusion particle analysis in biotherapeutics is a very important task with new challenges, but also possibilities with available techniques and the use of artificial intelligence.

## References

**1**. Walsh G. Biopharmaceutical benchmarks 2018. *Nat Biotechnol.* 2018;36(12):1136–1145.

**2**. Bak A, Friis KP, Wu Y, Ho RJY. Translating cell and gene biopharmaceutical products for health and market impact. Product scaling from clinical to marketplace: Lessons learned and future outlook. *J Pharm Sci.* 2019;108(10):3169–3175.

**3**. Narhi LO, Schmit J, Bechtold-Peters K, Sharma D. Classification of protein aggregates. *J Pharm Sci.* 2012;101(2):493–498.

**4**. Hawe A, Wiggenhorn M, van de Weert M, Garbe JHO, Mahler H-C, Jiskoot W. Forced degradation of therapeutic proteins. *J Pharm Sci.* 2012;101(3):895–913.

**5**. Samra HS, He F. Advancements in high throughput biophysical technologies: applications for characterization and screening during early formulation development of monoclonal antibodies. *Mol Pharm.* 2012;9(4):696–707.

**6**. Feng YW, Ooishi A, Honda S. Aggregation factor analysis for protein formulation by a systematic approach using FTIR, SEC and design of experiments techniques. *J Pharm Biomed Anal.* 2012;57:143–152.

**7**. Lowe D, Dudgeon K, Rouet R, Schofield P, Jermutus L, Christ D. Aggregation, stability, and formulation of human antibody therapeutics. *Adv Protein Chem Struct Biol.* 2011;84:41–61.

**8**. Filipe V, Jiskoot W, Basmeleh AH, Halim A, Schellekens H, Brinks V. Immunogenicity of different stressed IgG monoclonal antibody formulations in immune tolerant transgenic mice. *mAbs.* 2012;4(6):740–752.

**9**. Wang W, Singh SK, Li N, Toler MR, King KR, Nema S. Immunogenicity of protein aggregates – concerns and realities. *Int J Pharm.* 2012;431(1-2):1–11.

**10**. Moussa EM, Panchal JP, Moorthy BS, et al. Immunogenicity of therapeutic protein aggregates. *J Pharm Sci.* 2016;105(2):417–430.

**11**. Ratanji KD, Derrick JP, Dearman RJ, Kimber I. Immunogenicity of therapeutic proteins: influence of aggregation. *J Immunotoxicol.* 2014;11(2):99–109.

**12**. Ahmadi M, Bryson CJ, Cloake EA, et al. Small amounts of sub-visible aggregates enhance the immunogenic potential of monoclonal antibody therapeutics. *Pharm Res.* 2015;32(4):1383–1394.

**13**. Hoogendoorn KH, Crommelin DJA, Jiskoot W. Formulation of cell-based medicinal products: A question of life or death? *J Pharm Sci.* 2021;110(5):1885–1894.

**14**. Bulcha JT, Wang Y, Ma H, Tai PWL, Gao G. Viral vector platforms within the gene therapy landscape. *Signal Transduct Target Ther.* 2021;6(1):53.

**15**. Crommelin DJA, Volkin DB, Hoogendoorn KH, Lubiniecki AS, Jiskoot W. The science is there: Key considerations for stabilizing viral vector-based covid-19 vaccines. *J Pharm Sci.* 2021;110(2):627–634.

**16**. Voysey M, Costa Clemens SA, Madhi SA, et al. Single-dose administration and the influence of the timing of the booster dose on immunogenicity and efficacy of ChAdOx1 nCoV-19 (AZD1222) vaccine: a pooled analysis of four randomised trials. *Lancet.* 2021;397(10277):881–891.

**17**. Sadoff J, Le Gars M, Shukarev G, et al. Interim results of a phase 1–2a trial of Ad26.COV2.S covid-19 vaccine. *N Engl J Med.* 2021;384(19):1824–1835.

**18**. Ungerechts G, Bossow S, Leuchs B, et al. Moving oncolytic viruses into the clinic: clinical-grade production, purification, and characterization of diverse oncolytic viruses. *Mol Ther Methods Clin Dev.* 2016;3:16018.

**19**. Merten O-W, Al-Rubeai M. *Viral Vectors for Gene Therapy*. Humana Press; 2011.

**20**. Gimpel AL, Katsikis G, Sha S, et al. Analytical methods for process and product characterization of recombinant adeno-associated virus-based gene therapies. *Mol Ther Methods Clin Dev.* 2021;20:740–754.

**21**. Le DT, Müller KM. In vitro assembly of virus-like particles and their applications. *Life (Basel).* 2021;11(4):334.

**22**. Nooraei S, Bahrulolum H, Hoseini ZS, et al. Virus-like particles: preparation, immunogenicity and their roles as nanovaccines and drug nanocarriers. *J Nanobiotechnology.* 2021;19(1):59.

**23**. Mathaes R, Narhi L, Hawe A, et al. Phase-appropriate application of analytical methods to monitor subvisible particles across the biotherapeutic drug product life cycle. *AAPS J.* 2019;22(1):1.

**24**. Kretsinger J, Frantz N, Hart SA, et al. Expectations for phase-appropriate drug substance and drug product specifications for early-stage protein therapeutics. *J Pharm Sci.* 2019;108(4):1442–1452.

**25**. Hubert M, Yang DT, Kwok SC, et al. A multicompany assessment of submicron particle levels by NTA and RMM in a wide range of late-phase clinical and commercial biotechnology-derived protein products. *J Pharm Sci.* 2020;109(1):830–844.

**26**. Ríos Quiroz A, Lamerz J, Da Cunha T, et al. Factors governing the precision of subvisible particle measurement methods - A case study with a low-concentration therapeutic protein product in a prefilled syringe. *Pharm Res.* 2016;33(2):450–461.

**27**. Ríos Quiroz A, Finkler C, Huwyler J, Mahler H-C, Schmidt R, Koulov AV. Factors governing the accuracy of subvisible particle counting methods. *J Pharm Sci.* 2016;105(7):2042–2052.

**28**. Ripple DC, Montgomery CB, Hu Z. An interlaboratory comparison of sizing and counting of subvisible particles mimicking protein aggregates. *J Pharm Sci.* 2015;104(2):666–677.

**29**. Kiyoshi M, Shibata H, Harazono A, et al. Collaborative study for analysis of subvisible particles using flow imaging and light obscuration: Experiences in japanese biopharmaceutical consortium. *J Pharm Sci.* 2019;108(2):832–841.

**30**. Zhao H, Ghirlando R, Alfonso C, et al. A multilaboratory comparison of calibration accuracy and the performance of external references in analytical ultracentrifugation. *PLoS ONE.* 2015;10(5):e0126420.

**31**. Zölls S, Tantipolphan R, Wiggenhorn M, et al. Particles in therapeutic protein formulations, Part 1: overview of analytical methods. *J Pharm Sci.* 2012;101(3):914–935.

**32**. Weinbuch D, Jiskoot W, Hawe A. Light obscuration measurements of highly viscous solutions: sample pressurization overcomes underestimation of subvisible particle counts. *AAPS J.* 2014;16(5):1128–1131.

**33**. Gross-Rother J, Blech M, Preis E, Bakowsky U, Garidel P. Particle detection and characterization for biopharmaceutical applications: Current principles of established and alternative techniques. *Pharmaceutics.* 2020;12(11):1112.

**34**. Burg TP, Godin M, Knudsen SM, et al. Weighing of biomolecules, single cells and single nanoparticles in fluid. *Nature.* 2007;446(7139):1066–1069.

**35**. Weinbuch D, Zölls S, Wiggenhorn M, et al. Micro-flow imaging and resonant mass measurement (Archimedes) – complementary methods to quantitatively differentiate protein particles and silicone oil droplets. *J Pharm Sci.* 2013;102(7):2152–2165.

**36**. Dextras P, Burg TP, Manalis SR. Integrated measurement of the mass and surface charge of discrete microparticles using a suspended microchannel resonator. *Anal Chem.* 2009;81(11):4517–4523.

**37**. Strehl R, Rombach-Riegraf V, Diez M, et al. Discrimination between silicone oil droplets and protein aggregates in biopharmaceuticals: a novel multiparametric image filter for sub-visible particles in microflow imaging analysis. *Pharm Res.* 2012;29(2):594–602.

**38**. Patel AR, Lau D, Liu J. Quantification and characterization of micrometer and submicrometer subvisible particles in protein therapeutics by use of a suspended microchannel resonator. *Anal Chem.* 2012;84(15):6833–6840.

**39**. Barnard JG, Babcock K, Carpenter JF. Characterization and quantitation of aggregates and particles in interferon-β products: potential links between product quality attributes and immunogenicity. *J Pharm Sci.* 2013;102(3):915–928.

**40**. Felsovalyi F, Janvier S, Jouffray S, Soukiassian H, Mangiagalli P. Silicone-oil-based subvisible particles: their detection, interactions, and regulation in prefilled container closure systems for biopharmaceuticals. *J Pharm Sci.* 2012;101(12):4569–4583.

**41**. Rosenberg AS, Verthelyi D, Cherney BW. Managing uncertainty: a perspective on risk pertaining to product quality attributes as they bear on immunogenicity of therapeutic proteins. *J Pharm Sci.* 2012;101(10):3560–3567.

**42**. Fischer H, Polikarpov I, Craievich AF. Average protein density is a molecular-weight-dependent function. *Protein Sci.* 2004;13(10):2825–2828.

**43**. Folzer E, Khan TA, Schmidt R, et al. Determination of the density of protein particles using a suspended microchannel resonator. *J Pharm Sci.* 2015;104(12):4034–4040.

**44**. Krueger AB, Hadley J, Cheney PP, Markova N, Carpenter JF, Fradkin AH. Application of a best practice approach using resonant mass measurement for biotherapeutic product characterization. *J Pharm Sci.* 2019;108(5):1675–1685.

**45**. Barnard JG, Rhyner MN, Carpenter JF. Critical evaluation and guidance for using the Coulter method for counting subvisible particles in protein solutions. *J Pharm Sci.* 2012;101(1):140–153.

**46**. Stelzl A, Schneid S, Winter G. Application of Tunable Resistive Pulse Sensing for the quantification of submicron particles in pharmaceutical monoclonal antibody preparations. *J Pharm Sci.* 2021;110(11):3541–3545.

**47**. Helbig C, Ammann G, Menzen T, Friess W, Wuchner K, Hawe A. Backgrounded membrane imaging (BMI) for high-throughput characterization of subvisible particles during biopharmaceutical drug product development. *J Pharm Sci.* 2020;109(1):264–276.

**48**. Grabarek AD, Bozic U, Rousel J, et al. What makes polysorbate functional? Impact of polysorbate 80 grade and quality on IgG stability during mechanical stress. *J Pharm Sci.* 2020;109(1):871–880.

**49**. Wood CV, Razinkov VI, Qi W, Furst EM, Roberts CJ. A rapid, small-volume approach to evaluate protein aggregation at air-water interfaces. *J Pharm Sci.* 2021;110(3):1083–1092.

**50**. Das TK. Protein particulate detection issues in biotherapeutics development – current status. *AAPS PharmSciTech.* 2012;13(2):732–746.

**51**. Halo Labs. Protein aggregate identification with FMM: Rapidly distinguish protein from non-protein particles in biologic formulations (application note 7). Available at: https://www.halolabs.com/wp-content/uploads/2020/08/AN-7-Aura-Protein-ID.pdf. Accessed June 9, 2021.

**52**. Zuba-Surma EK, Kucia M, Abdel-Latif A, Lillard JW, Ratajczak MZ. The ImageStream System: a key step to a new era in imaging. *Folia Histochem Cytobiol.* 2007;45(4):279–290.

**53**. Probst C. Characterization of protein aggregates, silicone oil droplets, and protein-silicone interactions using imaging flow cytometry. *J Pharm Sci.* 2020;109(1):364–374.

**54**. Vanbillemont B, Carpenter JF, Probst C, Beer T de. The impact of formulation composition and process settings of traditional batch versus continuous freeze-drying on protein aggregation. *J Pharm Sci.* 2020;109(11):3308–3318.

**55**. Schuster J, Probst CE, Mahler H-C, Joerg S, Huwyler J, Mathaes R. Assessing particle formation of biotherapeutics in biological fluids. *J Pharm Sci.* 2021;110(4):1527–1532.

**56**. Dominical V, Samsel L, McCoy JP, Jr. Masks in imaging flow cytometry. *Methods.* 2017;112:9–17.

**57**. Sieracki C. Extending the limits: Oil immersion flow microscopy. *Am Lab.* 2018;50:18–21.

**58**. Krause N, Kuhn S, Frotscher E, et al. Oil-Immersion flow imaging microscopy for quantification and morphological characterization of submicron particles in biopharmaceuticals. *AAPS J.* 2021;23(1):13.

**59**. Umar M, Krause N, Hawe A, Simmel F, Menzen T. Towards quantification and differentiation of protein aggregates and silicone oil droplets in the low micrometer and submicrometer size range by using oil-immersion flow imaging microscopy and convolutional neural networks. *Eur J Pharm Biopharm.* 2021;169:97–102.

**60**. Lee S-H, Roichman Y, Yi G-R, et al. Characterizing and tracking single colloidal particles with video holographic microscopy. *Opt Express.* 2007;15(26):18275–18282.

**61**. Winters A, Cheong FC, Odete MA, et al. Quantitative differentiation of protein aggregates from other subvisible particles in viscous mixtures through holographic characterization. *J Pharm Sci.* 2020;109(8):2405–2412.

**62**. Kasimbeg PNO, Cheong FC, Ruffner DB, Blusewicz JM, Philips LA. Holographic characterization of protein aggregates in the presence of silicone oil and surfactants. *J Pharm Sci.* 2019;108(1):155–161.

**63**. Kamerzell TJ, Middaugh CR. Prediction machines: Applied machine learning for therapeutic protein design and development. *J Pharm Sci.* 2021;110(2):665–681.

**64**. Narayanan H, Dingfelder F, Butté A, Lorenzen N, Sokolov M, Arosio P. Machine learning for biologics: opportunities for protein engineering, developability, and formulation. *Trends Pharmacol Sci.* 2021;42(3):151–165.

**65**. Narayanan H, Dingfelder F, Condado Morales I, et al. Design of Biopharmaceutical Formulations Accelerated by Machine Learning. *Mol Pharm.* 2021;18(10):3843–3853.

**66**. Gambe-Gilbuena A, Shibano Y, Krayukhina E, Torisu T, Uchiyama S. Automatic identification of the stress sources of protein aggregates using flow imaging microscopy images. *J Pharm Sci.* 2020;109(1):614–623.

**67**. Calderon CP, Daniels AL, Randolph TW. Deep convolutional neural network analysis of flow imaging microscopy data to classify subvisible particles in protein formulations. *J Pharm Sci.* 2018;107(4):999–1008.

**68**. Sung JJ, Pardeshi NN, Mulder AM, et al. Transmission electron microscopy as an orthogonal method to characterize protein aggregates. *J Pharm Sci.* 2015;104(2):750–759.

**69**. Cavicchi RE, King J, Ripple DC. Measurement of average aggregate density by sedimentation and brownian motion analysis. *J Pharm Sci.* 2018;107(5):1304–1312.

**70**. Hong P, Koza S, Bouvier ESP. Size-exclusion chromatography for the analysis of protein biotherapeutics and their aggregates. *J Liq Chromatogr Relat Technol.* 2012;35(20):2923–2950.

**71**. Erickson HP. Size and shape of protein molecules at the nanometer level determined by sedimentation, gel filtration, and electron microscopy. *Biol Proced Online.* 2009;11:32–51.

**72**. Teraoka I. Calibration of retention volume in size exclusion chromatography by hydrodynamic radius. *Macromolecules.* 2004;37(17):6632–6639.

**73**. Mehn D, Caputo F, Rösslein M, et al. Larger or more? Nanoparticle characterisation methods for recognition of dimers. *RSC Adv.* 2017;7(44):27747–27754.

**74**. Maguire CM, Rösslein M, Wick P, Prina-Mello A. Characterisation of particles in solution - a perspective on light scattering and comparative technologies. *Sci Technol Adv Mater.* 2018;19(1):732–745.

**75**. Molodenskiy D, Shirshin E, Tikhonova T, Gruzinov A, Peters G, Spinozzi F. Thermally induced conformational changes and protein-protein interactions of bovine serum albumin in aqueous solution under different pH and ionic strengths as revealed by SAXS measurements. *Phys Chem Chem Phys.* 2017;19(26):17143–17155.

**76**. Some D, Amartely H, Tsadok A, Lebendiker M. Characterization of proteins by size-exclusion chromatography coupled to multi-angle light scattering (SEC-MALS). *J Vis Exp.* 2019(148).

**77**. Ruggeri FS, Šneideris T, Vendruscolo M, Knowles TPJ. Atomic force microscopy for single molecule characterisation of protein aggregation. *Arch Biochem Biophys.* 2019;664:134–148.

**78**. Demeule B, Palais C, Machaidze G, Gurny R, Arvinte T. New methods allowing the detection of protein aggregates: a case study on trastuzumab. *mAbs.* 2009;1(2):142–150.

**79**. DiMemmo LM, Cameron Varano A, Haulenbeek J, et al. Real-time observation of protein aggregates in pharmaceutical formulations using liquid cell electron microscopy. *Lab Chip.* 2017;17(2):315–322.

**80**. Maruno T, Watanabe H, Yoneda S, et al. Sweeping of adsorbed therapeutic protein on prefillable syringes promotes micron aggregate generation. *J Pharm Sci.* 2018;107(6):1521–1529.

**81**. Krayukhina E, Uchiyama S, Nojima K, Okada Y, Hamaguchi I, Fukui K. Aggregation analysis of pharmaceutical human immunoglobulin preparations using size-exclusion chromatography and analytical ultracentrifugation sedimentation velocity. *J Biosci Bioeng.* 2013;115(1):104–110.

**82**. Gandhi AV, Pothecary MR, Bain DL, Carpenter JF. Some lessons learned from a comparison between sedimentation velocity analytical ultracentrifugation and size exclusion chromatography to characterize and quantify protein aggregates. *J Pharm Sci.* 2017;106(8):2178–2186.

**83**. Liu J, Andya JD, Shire SJ. A critical review of analytical ultracentrifugation and field flow fractionation methods for measuring protein aggregation. *AAPS J.* 2006;8(3):E580-9.

**84**. Hawe A, Romeijn S, Filipe V, Jiskoot W. Asymmetrical flow field-flow fractionation method for the analysis of submicron protein aggregates. *J Pharm Sci.* 2012;101(11):4129–4139.

**85**. Harding SE, Gillis RB, Adams GG. Assessing sedimentation equilibrium profiles in analytical ultracentrifugation experiments on macromolecules: from simple average molecular weight analysis to molecular weight distribution and interaction analysis. *Biophys Rev.* 2016;8(4):299–308.

**86**. Wu D, Piszczek G. Standard protocol for mass photometry experiments. *Eur Biophys J.* 2021;50(3-4):403–409.

**87**. Brusotti G, Calleri E, Colombo R, Massolini G, Rinaldi F, Temporini C. Advances on size exclusion chromatography and applications on the analysis of protein biopharmaceuticals and protein aggregates: A mini review. *Chromatographia.* 2018;81(1):3–23.

**88**. Grabarek AD, Weinbuch D, Jiskoot W, Hawe A. Critical evaluation of microfluidic resistive pulse sensing for quantification and sizing of nanometer- and micrometer-sized particles in biopharmaceutical products. *J Pharm Sci.* 2019;108(1):563–573.

**89**. Filipe V, Hawe A, Carpenter JF, Jiskoot W. Analytical approaches to assess the degradation of therapeutic proteins. *Trends Analyt Chem.* 2013;49:118–125.

**90**. Gühlke M, Hecht J, Böhrer A, et al. Taking subvisible particle quantitation to the limit: Uncertainties and statistical challenges with ophthalmic products for intravitreal injection. *J Pharm Sci.* 2020;109(1):505–514.

**91**. Gross J, Sayle S, Karow AR, Bakowsky U, Garidel P. Nanoparticle tracking analysis of particle size and concentration detection in suspensions of polymer and protein samples: Influence of experimental and data evaluation parameters. *Eur J Pharm Biopharm.* 2016;104:30–41.

**92**. Defante AP, Vreeland WN, Benkstein KD, Ripple DC. Using image attributes to assure accurate particle size and count using nanoparticle tracking analysis. *J Pharm Sci.* 2018;107(5):1383–1391.

**93**. Zölls S, Gregoritza M, Tantipolphan R, et al. How subvisible particles become invisible-relevance of the refractive index for protein particle analysis. *J Pharm Sci.* 2013;102(5):1434–1446.

**94**. Ripple DC, Hu Z. Correcting the relative bias of light obscuration and flow imaging particle counters. *Pharm Res.* 2016;33(3):653–672.

**95**. Cavicchi RE, Carrier MJ, Cohen JB, et al. Particle shape effects on subvisible particle sizing measurements. *J Pharm Sci.* 2015;104(3):971–987.

**96**. Werk T, Volkin DB, Mahler H-C. Effect of solution properties on the counting and sizing of subvisible particle standards as measured by light obscuration and digital imaging methods. *Eur J Pharm Sci.* 2014;53:95–108.

**97**. Deiringer N, Haase C, Wieland K, Zahler S, Haisch C, Friess W. Finding the needle in the haystack: High-resolution techniques for characterization of mixed protein particles containing shed silicone rubber particles generated during pumping. *J Pharm Sci.* 2021;110(5):2093–2104.

**98**. Wuchner K, Büchler J, Spycher R, Dalmonte P, Volkin DB. Development of a microflow digital imaging assay to characterize protein particulates during storage of a high concentration IgG1 monoclonal antibody formulation. *J Pharm Sci.* 2010;99(8):3343–3361.

**99**. Hindelang F, Roggo Y, Zurbach R. Forensic investigation in the pharmaceutical industry: Identification procedure of visible particles in (drug) solutions and different containers by combining vibrational and X-ray spectroscopic techniques. *J Pharm Biomed Anal.* 2018;148:334–349.

**100**. Guibert D de, Hennetier M, Martin F, et al. Flow process and heating conditions modulate the characteristics of whey protein aggregates. *J Food Eng.* 2020;264:109675.

**101**. Stetefeld J, McKenna SA, Patel TR. Dynamic light scattering: a practical guide and applications in biomedical sciences. *Biophys Rev.* 2016;8(4):409–427.

**102**. Daniels AL, Calderon CP, Randolph TW. Machine learning and statistical analyses for extracting and characterizing "fingerprints" of antibody aggregation at container interfaces from flow microscopy images. *Biotechnol Bioeng.* 2020(117):3322–3335.

**103**. Jones MT, Mahler H-C, Yadav S, et al. Considerations for the use of polysorbates in biopharmaceuticals. *Pharm Res.* 2018;35(8):148.

**104**. Tomlinson A, Demeule B, Lin B, Yadav S. Polysorbate 20 degradation in biopharmaceutical formulations: quantification of free fatty acids, characterization of particulates, and insights into the degradation mechanism. *Mol Pharm.* 2015;12(11):3805–3815.

**105**. Kishore RSK, Kiese S, Fischer S, Pappenberger A, Grauschopf U, Mahler H-C. The degradation of polysorbates 20 and 80 and its potential impact on the stability of biotherapeutics. *Pharm Res.* 2011;28(5):1194–1210.

**106**. Doshi N, Demeule B, Yadav S. Understanding particle formation: Solubility of free fatty acids as polysorbate 20 degradation byproducts in therapeutic monoclonal antibody formulations. *Mol Pharm.* 2015;12(11):3792–3804.

**107**. Dixit N, Salamat-Miller N, Salinas PA, Taylor KD, Basu SK. Residual host cell protein promotes polysorbate 20 degradation in a sulfatase drug product leading to free fatty acid particles. *J Pharm Sci.* 2016;105(5):1657–1666.

**108**. Labrenz SR. Ester hydrolysis of polysorbate 80 in mAb drug product: evidence in support of the hypothesized risk after the observation of visible particulate in mAb formulations. *J Pharm Sci.* 2014;103(8):2268–2277.

**109**. Zhang L, Yadav S, Demeule B, Wang YJ, Mozziconacci O, Schöneich C. Degradation Mechanisms of Polysorbate 20 Differentiated by 18 O-labeling and Mass Spectrometry. *Pharm Res.* 2017;34(1):84–100.

**110**. Cao X, Fesinmeyer RM, Pierini CJ, et al. Free fatty acid particles in protein formulations, part 1: microspectroscopic identification. *J Pharm Sci.* 2015;104(2):433–446.

**111**. Dwivedi M, Blech M, Presser I, Garidel P. Polysorbate degradation in biotherapeutic formulations: Identification and discussion of current root causes. *Int J Pharm.* 2018;552(1-2):422–436.

**112**. Saggu M, Liu J, Patel A. Identification of subvisible particles in biopharmaceutical formulations using Raman spectroscopy provides insight into polysorbate 20 degradation pathway. *Pharm Res.* 2015;32(9):2877–2888.

**113**. Saggu M, Demeule B, Jiang L, et al. Extended characterization and impact of visible fatty acid particles - A case study with a mAb product. *J Pharm Sci.* 2021;110(3):1093–1102.

**114**. Allmendinger A, Lebouc V, Bonati L, Woehr A, Kishore RSK, Abstiens K. Glass leachables as a nucleation factor for free fatty acid particle formation in biopharmaceutical formulations. *J Pharm Sci.* 2021;110(2):785–795.

**115**. Lee JC, Timasheff SN. The stabilization of proteins by sucrose. *J Biol Chem.* 1981;256(14):7193–7201.

**116**. Rowe RC, Sheskey PJ, Quinn ME, eds. *Handbook of pharmaceutical excipients, 6th ed.,* London: APhA (PhP) Pharmaceutical Press; 2009.

**117**. Weinbuch D, Cheung JK, Ketelaars J, et al. Nanoparticulate impurities in pharmaceutical-grade sugars and their interference with light scattering-based analysis of protein formulations. *Pharm Res.* 2015;32(7):2419–2427.

**118**. Weinbuch D, Ruigrok M, Jiskoot W, Hawe A. Nanoparticulate impurities isolated from pharmaceutical-grade sucrose are a potential threat to protein stability. *Pharm Res.* 2017;34(12):2910–2921.

**119**. Langille SE. Particulate matter in injectable drug products. *PDA J Pharm Sci Technol.* 2013;67(3):186–200.

**120**. Bukofzer S, Ayres J, Chavez A, et al. Industry perspective on the medical risk of visible particles in injectable drug products. *PDA J Pharm Sci Technol.* 2015;69(1):123–139.

**121**. Sacha GA, Saffell-Clemmer W, Abram K, Akers MJ. Practical fundamentals of glass, rubber, and plastic sterile packaging systems. *Pharm Dev Technol.* 2010;15(1):6–34.

**122**. Krayukhina E, Yokoyama M, Hayashihara KK, et al. An assessment of the ability of submicron- and micron-size silicone oil droplets in dropped prefillable syringes to invoke early- and late-stage immune responses. *J Pharm Sci.* 2019;108(7):2278–2287.

**123**. Chisholm CF, Baker AE, Soucie KR, Torres RM, Carpenter JF, Randolph TW. Silicone oil microdroplets can induce antibody responses against recombinant murine growth hormone in mice. *J Pharm Sci.* 2016;105(5):1623–1632.

**124**. Ueda T, Nakamura K, Abe Y, Carpenter JF. Effects of product handling parameters on particle levels in a commercial factor VIII product: Impacts and mitigation. *J Pharm Sci.* 2019;108(1):775–786.

**125**. Fradkin AH, Carpenter JF, Randolph TW. Glass particles as an adjuvant: A model for adverse immunogenicity of therapeutic proteins. *J Pharm Sci.* 2011;100(11):4953–4964.

**126**. Doessegger L, Mahler H-C, Szczesny P, et al. The potential clinical relevance of visible particles in parenteral drugs. *J Pharm Sci.* 2012;101(8):2635–2644.

**127**. Srinivasan C, Ma Y, Liu Y, et al. Quality attributes and evaluation of pharmaceutical glass containers for parenterals. *Int J Pharm.* 2019;568:118510.

**128**. Rech J, Fradkin A, Krueger A, Kraft C, Paskiet D. Evaluation of particle techniques for the characterization of subvisible particles from elastomeric closure components. *J Pharm Sci.* 2020;109(5):1725–1735.

**129**. Joh NH, Thomas L, Christian TR, et al. Silicone oil particles in prefilled syringes with human monoclonal antibody, representative of real-world drug products, did not increase immunogenicity in in vivo and in vitro model systems. *J Pharm Sci.* 2020;109(1):845–853.

**130**. Chisholm CF, Nguyen BH, Soucie KR, Torres RM, Carpenter JF, Randolph TW. In vivo analysis of the potency of silicone oil microdroplets as immunological adjuvants in protein formulations. *J Pharm Sci.* 2015;104(11):3681–3690.

**131**. Sharma A, Kumar N, Bandello F, Loewenstein A, Freund KB. Understanding intravitreal silicone oil droplets due to intravitreal injections. *Retina.* 2019;39(7):1233–1235.

**132**. Gómez-Mariscal M, Díez-Álvarez L. Silicone oil droplets after intravitreal injections: An uncomfortable adverse effect in our consultations. *Arch Soc Esp Oftamol (Engl Ed).* 2020;95(6):261–262.

**133**. Thompson JT. Prospective study of silicone oil microdroplets in eyes receiving intravitreal anti-vascular endothelial growth factor therapy in 3 different syringes. *Ophthalmol Retina.* 2021;5(3):234–240.

**134**. Saggu M, Patel AR, Koulis T. A random forest approach for counting silicone oil droplets and protein particles in antibody formulations using flow microscopy. *Pharm Res.* 2017;34(2):479–491.

**135**. Chen XG, Graužinytė M, van der Vaart AW, Boll B. Applying pattern recognition as a robust approach for silicone oil droplet identification in flow-microscopy images of protein formulations. *J Pharm Sci.* 2021;110(4):1643–1651.

**136**. Sharma DK, King D, Oma P, Merchant C. Micro-flow imaging: Flow microscopy applied to sub-visible particulate analysis in protein formulations. *AAPS J.* 2010;12(3):455–464.

**137**. Akhunzada ZS, Hubert M, Sahin E, Pratt J. Separation, characterization and discriminant analysis of subvisible particles in biologics formulations. *Curr Pharm Biotechnol.* 2019;20(3):232–244.

**138**. Probst C, Zayats A, Venkatachalam V, Davidson B. Advanced characterization of silicone oil droplets in protein therapeutics using artificial intelligence analysis of imaging flow cytometry data. *J Pharm Sci.* 2020;109(10):2996–3005.

**139**. Ludwig DB, Trotter JT, Gabrielson JP, Carpenter JF, Randolph TW. Flow cytometry: a promising technique for the study of silicone oil-induced particulate formation in protein formulations. *Anal Biochem.* 2011;410(2):191–199.

**140**. Teska BM, Brake JM, Tronto GS, Carpenter JF. Aggregation and particle formation of therapeutic proteins in contact with a novel fluoropolymer surface versus siliconized surfaces: Effects of agitation in vials and in prefilled syringes. *J Pharm Sci.* 2016;105(7):2053–2065.

**141**. Cao X, Wen Z-Q, Vance A, Torraca G. Raman microscopic applications in the biopharmaceutical industry: in situ identification of foreign particulates inside glass containers with aqueous formulated solutions. *Appl Spectrosc.* 2009;63(7):830–834.

**142**. Grapentin C, Müller C, Kishore RSK, et al. Protein-polydimethylsiloxane particles in liquid vial monoclonal antibody formulations containing Poloxamer 188. *J Pharm Sci.* 2020;109(8):2393–2404.

**143**. Lankers M, Munhall J, Valet O. Differentiation between foreign particulate matter and silicone oil induced protein aggregation in drug solutions by automated raman spectroscopy. *Microsc Microanal.* 2008;14S2:1612–1613.

**144**. Li GG, Cao S, Jiao N, Wen Z-Q. Classification of glass particles in parenteral product vials by visual, microscopic, and spectroscopic methods. *PDA J Pharm Sci Technol.* 2014;68(4):362–372.

**145**. Ditter D, Nieto A, Mahler H-C, et al. Evaluation of glass delamination risk in pharmaceutical 10 mL/10R vials. *J Pharm Sci.* 2018;107(2):624–637.

**146**. Iacocca RG, Toltl N, Allgeier M, et al. Factors affecting the chemical durability of glass used in the pharmaceutical industry. *AAPS PharmSciTech.* 2010;11(3):1340–1349.

**147**. Ogawa T, Miyajima M, Wakiyama N, Terada K. Effects of phosphate buffer in parenteral drugs on particle formation from glass vials. *Chem Pharm Bull.* 2013;61(5):539–545.

**148**. Jiang G, Goss M, Li G, et al. Novel mechanism of glass delamination in type 1A borosilicate vials containing frozen protein formulations. *PDA J Pharm Sci Technol.* 2013;67(4):323–335.

**149**. Ratnaswamy G, Hair A, Li G, et al. A case study of nondelamination glass dissolution resulting in visible particles: implications for neutral pH formulations. *J Pharm Sci.* 2014;103(4):1104–1114.

**150**. Cook M, Chauhan A. Clinical application of oncolytic viruses: a systematic review. *Int J Mol Sci.* 2020;21(20):7505.

**151**. Niu Q, Ma L, Zhu S, et al. Quantitative assessment of the physical virus titer and purity by ultrasensitive flow virometry. *Angew Chem Int Ed Engl.* 2021;60(17):9351–9356.

**152**. Segura MM, Mangion M, Gaillet B, Garnier A. New developments in lentiviral vector design, production and purification. *Expert Opin Biol Ther.* 2013;13(7):987–1011.

**153**. Moreira AS, Cavaco DG, Faria TQ, Alves PM, Carrondo MJT, Peixoto C. Advances in lentivirus purification. *Biotechnol J.* 2021;16(1):e2000019.

**154**. Roldão A, Silva AC, Mellado MCM, Alves PM, Carrondo MJT. Viruses and Virus-Like Particles in Biotechnology: Fundamentals and Applications. *Comprehensive Biotechnology*. 2011:625–49.

**155**. Heider S, Metzner C. Quantitative real-time single particle analysis of virions. *Virology.* 2014;462-463:199–206.

**156**. Akpinar F, Yin J. Characterization of vesicular stomatitis virus populations by tunable resistive pulse sensing. *J Virol Methods.* 2015;218:71–76.

**157**. Maruno T, Usami K, Ishii K, Torisu T, Uchiyama S. Comprehensive size distribution and composition analysis of adeno-associated virus vector by multiwavelength sedimentation velocity analytical ultracentrifugation. *J Pharm Sci.* 2021;110(10):3375–3384.

**158**. Turkki V, Alppila E, Ylä-Herttuala S, Lesch HP. Experimental evaluation of an interferometric light microscopy particle counter for titering and characterization of virus preparations. *Viruses.* 2021;13(5):939.

**159**. Lippé R. Flow virometry: a powerful tool to functionally characterize viruses. *J Virol.* 2018;92(3):1–11.

**160**. Wu D, Hwang P, Li T, Piszczek G. Rapid characterization of AAV gene therapy vectors by mass photometry. *bioRxiv.* 2021;71.

**161**. Wörner TP, Shamorkina TM, Snijder J, Heck AJR. Mass spectrometry-based structural virology. *Anal Chem.* 2021;93(1):620–640.

**162**. Milewska A, Ner-Kluza J, Dabrowska A, Bodzon-Kulakowska A, Pyrc K, Suder P. Mass spectrometry in virological sciences. *Mass Spectrom Rev.* 2020;39(5-6):499–522.

**163**. Dominguez-Medina S, Fostner S, Defoort M, et al. Neutral mass spectrometry of virus capsids above 100 megadaltons with nanomechanical resonators. *Science.* 2018;362(6417):918–922.

**164**. Wörner TP, Snijder J, Bennett A, Agbandje-McKenna M, Makarov AA, Heck AJR. Resolving heterogeneous macromolecular assemblies by Orbitrap-based single-particle charge detection mass spectrometry. *Nat Methods.* 2020;17(4):395–398.

**165**. Wei Z, McEvoy M, Razinkov V, et al. Biophysical characterization of influenza virus subpopulations using field flow fractionation and multiangle light scattering: correlation of particle counts, size distribution and infectivity. *J Virol Methods.* 2007;144(1-2):122–132.

**166**. Bagrov DV, Glukhov GS, Moiseenko AV, et al. Structural characterization of β-propiolactone inactivated severe acute respiratory syndrome coronavirus 2 (SARS-CoV-2) particles. *Microsc Res Tech.* 2021:1–8.

**167**. Bousse T, Shore DA, Goldsmith CS, et al. Quantitation of influenza virus using field flow fractionation and multi-angle light scattering for quantifying influenza A particles. *J Virol Methods.* 2013;193(2):589–596.

**168**. Navarro Sanchez ME, Soulet D, Bonnet E, et al. Rabies vaccine characterization by nanoparticle tracking analysis. *Sci Rep.* 2020;10(1):8149.

**169**. Transfiguracion J, Manceur AP, Petiot E, Thompson CM, Kamen AA. Particle quantification of influenza viruses by high performance liquid chromatography. *Vaccine.* 2015;33(1):78–84.

**170**. Nikiforov VN, Vinogradov SE, Ivanov AV, et al. Application of laser correlation spectroscopy for measuring virus size. *Bull Exp Biol Med.* 2016;161(1):88–91.

**171**. Yang L, Yamamoto T. Quantification of virus particles using nanopore-based resistive-pulse sensing techniques. *Front Microbiol.* 2016;7:1500.

**172**. Herzog C, Hartmann K, Künzi V, et al. Eleven years of Inflexal V-a virosomal adjuvanted influenza vaccine. *Vaccine.* 2009;27(33):4381–4387.

**173**. Wang R, Pan W, Jin L, et al. Human papillomavirus vaccine against cervical cancer: Opportunity and challenge. *Cancer Lett.* 2020;471:88–102.

**174**. Bovier PA. Epaxal: a virosomal vaccine to prevent hepatitis A infection. *Expert Rev Vaccines.* 2008;7(8):1141–1150.

**175**. Gause KT, Wheatley AK, Cui J, Yan Y, Kent SJ, Caruso F. Immunological principles guiding the rational design of particles for vaccine delivery. *ACS Nano.* 2017;11(1):54–68.

**176**. Hirsch J, Faber BW, Crowe JE, Jr., Verstrepen B, Cornelissen G. E. coli production process yields stable dengue 1 virus-sized particles (VSPs). *Vaccine.* 2020;38(17):3305–3312.

**177**. Steppert P, Burgstaller D, Klausberger M, Tover A, Berger E, Jungbauer A. Quantification and characterization of virus-like particles by size-exclusion chromatography and nanoparticle tracking analysis. *J Chromatogr A.* 2017;1487:89–99.

**178**. Hosseini SN, Sarvari T, Bashiri G, Khatami M, Shojaosadati SA. Assessing virus like particles formation and r-HBsAg aggregation during large scale production of recombinant hepatitis B surface antigen from Pichia pastoris. *Int J Biol Macromol.* 2019;139:697–711.

**179**. Somasundaram B, Chang C, Fan YY, Lim P-Y, Cardosa J, Lua L. Characterizing Enterovirus 71 and Coxsackievirus A16 virus-like particles production in insect cells. *Methods.* 2016;95:38–45.

**180**. Chen Y, Zhang Y, Quan C, et al. Aggregation and antigenicity of virus like particle in salt solution – A case study with hepatitis B surface antigen. *Vaccine.* 2015;33(35):4300–4306.

**181**. Shi L, Sanyal G, Ni A, et al. Stabilization of human papillomavirus virus-like particles by non-ionic surfactants. *J Pharm Sci.* 2005;94(7):1538–1551.

**182**. Zhang X, Wei M, Pan H, et al. Robust manufacturing and comprehensive characterization of recombinant hepatitis E virus-like particles in Hecolin(®). *Vaccine.* 2014;32(32):4039–4050.

**183**. Reiter K, Aguilar PP, Wetter V, Steppert P, Tover A, Jungbauer A. Separation of virus-like particles and extracellular vesicles by flow-through and heparin affinity chromatography. *J Chromatogr A.* 2019;1588:77–84.

**184**. Sherry L, Grehan K, Snowden JS, et al. Comparative molecular biology approaches for the production of Poliovirus virus-like particles using Pichia pastoris. *mSphere.* 2020;5(2):e00838-19.

**185**. McCraw DM, Gallagher JR, Torian U, et al. Structural analysis of influenza vaccine virus-like particles reveals a multicomponent organization. *Sci Rep.* 2018;8(1):10342.

**186**. Havlik M, Marchetti-Deschmann M, Friedbacher G, et al. Comprehensive size-determination of whole virus vaccine particles using gas-phase electrophoretic mobility macromolecular analyzer, atomic force microscopy, and transmission electron microscopy. *Anal Chem.* 2015;87(17):8657–8664.

**187**. Wetzel D, Chan J-A, Suckow M, et al. Display of malaria transmission-blocking antigens on chimeric duck hepatitis B virus-derived virus-like particles produced in Hansenula polymorpha. *PLoS ONE.* 2019;14(9):e0221394.

**188**. Wu Y, Abraham D, Carta G. Particle size effects on protein and virus-like particle adsorption on perfusion chromatography media. *J Chromatogr A.* 2015;1375:92–100.

**189**. González-Domínguez I, Puente-Massaguer E, Cervera L, Gòdia F. Quality assessment of virus-like particles at single particle level: a comparative study. *Viruses.* 2020;12(2):223.

**190**. Shiri F, Petersen KE, Romanov V, Zou Q, Gale BK. Characterization and differential retention of Q beta bacteriophage virus-like particles using cyclical electrical field-flow fractionation and asymmetrical flow field-flow fractionation. *Anal Bioanal Chem.* 2020;412(7):1563–1572.

**191**. Ladd Effio C, Oelmeier SA, Hubbuch J. High-throughput characterization of virus-like particles by interlaced size-exclusion chromatography. *Vaccine.* 2016;34(10):1259–1267.

**192**. Mohr J, Chuan YP, Wu Y, Lua LHL, Middelberg APJ. Virus-like particle formulation optimization by miniaturized high-throughput screening. *Methods.* 2013;60(3):248–256.

**193**. Chen S, Tam YYC, Lin PJC, Sung MMH, Tam YK, Cullis PR. Influence of particle size on the in vivo potency of lipid nanoparticle formulations of siRNA. *J Control Release.* 2016;235:236–244.

**194**. Sato Y, Note Y, Maeki M, et al. Elucidation of the physicochemical properties and potency of siRNA-loaded small-sized lipid nanoparticles for siRNA delivery. *J Control Release.* 2016;229:48–57.

**195**. Zhang N-N, Li X-F, Deng Y-Q, et al. A thermostable mRNA vaccine against COVID-19. *Cell.* 2020;182(5):1271-1283.e16.

**196**. Vitorino C, Carvalho FA, Almeida AJ, Sousa JJ, Pais AACC. The size of solid lipid nanoparticles: an interpretation from experimental design. *Colloids Surf B Biointerfaces.* 2011;84(1):117–130.

**197**. Caputo F, Arnould A, Bacia M, et al. Measuring particle size distribution by asymmetric flow field flow fractionation: a powerful method for the preclinical characterization of lipid-based nanoparticles. *Mol Pharm.* 2019;16(2):756–767.

**198**. Zhang J, Haas RM, Leone AM. Polydispersity characterization of lipid nanoparticles for siRNA delivery using multiple detection size-exclusion chromatography. *Anal Chem.* 2012;84(14):6088–6096.

**199**. Henrickson A, Kulkarni JA, Zaifman J, Gorbet GE, Cullis PR, Demeler B. Density matching multi-wavelength analytical ultracentrifugation to measure drug loading of lipid nanoparticle formulations. *ACS Nano.* 2021;15(3):5068–5076.

**200**. Mildner R, Hak S, Parot J, et al. Improved multidetector asymmetrical-flow field-flow fractionation method for particle sizing and concentration measurements of lipid-based nanocarriers for RNA delivery. *Eur J Pharm Biopharm.* 2021;163:252–265.

**201**. Ayat NR, Sun Z, Sun D, et al. Formulation of biocompatible targeted ECO/siRNA nanoparticles with long-term stability for clinical translation of RNAi. *Nucleic Acid Ther.* 2019;29(4):195–207.

**202**. Ball RL, Bajaj P, Whitehead KA. Achieving long-term stability of lipid nanoparticles: examining the effect of pH, temperature, and lyophilization. *Int J Nanomedicine.* 2017;12:305–315.

**203**. Suzuki Y, Hyodo K, Tanaka Y, Ishihara H. siRNA-lipid nanoparticles with long-term storage stability facilitate potent gene-silencing in vivo. *J Control Release.* 2015;220(Pt A):44–50.

**204**. Gilham DE, Debets R, Pule M, Hawkins RE, Abken H. CAR-T cells and solid tumors: tuning T cells to challenge an inveterate foe. *Trends Mol Med.* 2012;18(7):377–384.

**205**. Pavillon N, Kühn J, Moratal C, et al. Early cell death detection with digital holographic microscopy. *PLoS ONE.* 2012;7(1):e30912.

**206**. Gómez-Angelats M, Cidlowski JA. Cell volume control and signal transduction in apoptosis. *Toxicol Pathol.* 2002;30(5):541–551.

**207**. USP 37. <1044> Cryopreservation of cells. In: United States Pharmacopeial Convention, ed. *The United States Pharmacopeia 37 (USP37). The national formulary 32 (NF32), 1st ed.,* Rockville, Md.; 2014.

**208**. Coulter WH. *High speed automatic blood cell counter and cell size analyzer*; 1956.

**209**. Casula E, Asuni GP, Sogos V, Fadda S, Delogu F, Cincotti A. Osmotic behaviour of human mesenchymal stem cells: Implications for cryopreservation. *PLoS ONE.* 2017;12(9):e0184180.

**210**. Vian AM, Higgins AZ. Membrane permeability of the human granulocyte to water, dimethyl sulfoxide, glycerol, propylene glycol and ethylene glycol. *Cryobiology.* 2014;68(1):35–42.

**211**. Fang C, Ji F, Shu Z, Gao D. Determination of the temperature-dependent cell membrane permeabilities using microfluidics with integrated flow and temperature control. *Lab Chip.* 2017;17(5):951–960.

**212**. Peckys D, Mazur P. Regulatory volume decrease in COS-7 cells at 22 °C and its influence on the Boyle van't Hoff relation and the determination of the osmotically inactive volume. *Cryobiology.* 2012;65(1):74–78.

**213**. Shu Z, Hughes SM, Fang C, et al. A study of the osmotic characteristics, water permeability, and cryoprotectant permeability of human vaginal immune cells. *Cryobiology.* 2016;72(2):93–99.

**214**. Spindler R, Rosenhahn B, Hofmann N, Glasmacher B. Video analysis of osmotic cell response during cryopreservation. *Cryobiology.* 2012;64(3):250–260.

**215**. Singh H, Figliola MJ, Dawson MJ, et al. Manufacture of clinical-grade CD19-specific T cells stably expressing chimeric antigen receptor using Sleeping Beauty system and artificial antigen presenting cells. *PLoS ONE.* 2013;8(5):e64138.

**216**. Wiesinger M, Stoica D, Roessner S, et al. Good Manufacturing Practice-Compliant production and lot-release of Ex Vivo expanded regulatory T Cells as basis for treatment of patients with autoimmune and inflammatory disorders. *Front Immunol.* 2017;8:1371.

**217**. Cunha B, Aguiar T, Silva MM, et al. Exploring continuous and integrated strategies for the up- and downstream processing of human mesenchymal stem cells. *J Biotechnol.* 2015;213:97–108.

**218**. Cadena-Herrera D, Esparza-De Lara JE, Ramírez-Ibañez ND, et al. Validation of three viable-cell counting methods: Manual, semi-automated, and automated. *Biotechnol Rep (Amst).* 2015;7:9–16.

**219**. Germann A, Oh YJ, Schmidt T, Schon U, Zimmermann H, Briesen H von. Temperature fluctuations during deep temperature cryopreservation reduce PBMC recovery, viability and T-cell function. *Cryobiology.* 2013;67(2):193–200.

**220**. Sediq AS, Klem R, Nejadnik MR, Meij P, Jiskoot W. Label-free, flow-imaging methods for determination of cell concentration and viability. *Pharm Res.* 2018;35(8):150.

**221**. Grabarek AD, Jiskoot W, Hawe A, Pike-Overzet K, Menzen T. Forced degradation of cell-based medicinal products guided by flow imaging microscopy: Explorative studies with Jurkat cells. *Eur J Pharm Biopharm.* 2021;167:38–47.

**222**. Castro VIB, Craveiro R, Silva JM, Reis RL, Paiva A, C Duarte AR. Natural deep eutectic systems as alternative nontoxic cryoprotective agents. *Cryobiology.* 2018;83:15–26.

**223**. Pi C-H, Hornberger K, Dosa P, Hubel A. Understanding the freezing responses of T cells and other subsets of human peripheral blood mononuclear cells using DSMO-free cryoprotectants. *Cytotherapy.* 2020;22(5):291–300.

**224**. Brauchle E, Thude S, Brucker SY, Schenke-Layland K. Cell death stages in single apoptotic and necrotic cells monitored by Raman microspectroscopy. *Sci Rep.* 2014;4:4698.

**225**. Mock U, Nickolay L, Philip B, et al. Automated manufacturing of chimeric antigen receptor T cells for adoptive immunotherapy using CliniMACS prodigy. *Cytotherapy.* 2016;18(8):1002–1011.

**226**. Ichimura T, Chiu L-d, Fujita K, et al. Non-label immune cell state prediction using Raman spectroscopy. *Sci Rep.* 2016;6:37562.

**227**. McReynolds N, Cooke FGM, Chen M, Powis SJ, Dholakia K. Multimodal discrimination of immune cells using a combination of Raman spectroscopy and digital holographic microscopy. *Sci Rep.* 2017;7:43631.

**228**. Akagi Y, Mori N, Kawamura T, Takayama Y, Kida YS. Non-invasive cell classification using the Paint Raman Express Spectroscopy System (PRESS). *Sci Rep.* 2021;11(1):8818.

**229**. Gavgiotaki E, Filippidis G, Zerva I, et al. Detection of the T cell activation state using nonlinear optical microscopy. *J Biophotonics.* 2019;12(3):e201800277.

**230**. Vollrath I, Mathaes R, Sediq AS, et al. Subvisible particulate contamination in cell therapy products-can we distinguish? *J Pharm Sci.* 2020;109(1):216–219.

**231**. Grabarek AD, Senel E, Menzen T, et al. Particulate impurities in cell-based medicinal products traced by flow imaging microscopy combined with deep learning for image analysis. *Cytotherapy.* 2021;23(4):339–347.

**232**. Morales JMM, Münch N, Peter K, et al. Automated clinical grade expansion of regulatory T cells in a fully closed system. *Front Immunol.* 2019;10:38.

**233**. Baradez M-O, Biziato D, Hassan E, Marshall D. Application of Raman spectroscopy and univariate modelling as a process analytical technology for cell therapy bioprocessing. *Front Med (Lausanne).* 2018;5:47.

**234**. Dhondalay GK, Lawrence K, Ward S, Ball G, Hoare M. Relationship between preparation of cells for therapy and cell quality using artificial neural network analysis. *Artif Intell Med.* 2014;62(2):119–127.

**235**. Yu G, Li R, Hubel A. Interfacial interactions of sucrose during cryopreservation detected by Raman spectroscopy. *Langmuir.* 2019;35(23):7388–7395.

**236**. Yu G, Yap YR, Pollock K, Hubel A. Characterizing intracellular ice formation of lymphoblasts using low-temperature Raman spectroscopy. *Biophys J.* 2017;112(12):2653–2663.

**237**. Hornberger K, Li R, Duarte ARC, Hubel A. Natural deep eutectic systems for nature-inspired cryopreservation of cells. *AIChE J.* 2021;67(2):e17085.

**238**. Pi C-H, Yu G, Dosa PI, Hubel A. Characterizing modes of action and interaction for multicomponent osmolyte solutions on Jurkat cells. *Biotechnol Bioeng.* 2019;116(3):631–643.

**239**. Meneghel J, Kilbride P, Morris JG, Fonseca F. Physical events occurring during the cryopreservation of immortalized human T cells. *PLoS ONE.* 2019;14(5):e0217304.

**240**. Murray KA, Gibson MI. Post-thaw culture and measurement of total cell recovery is crucial in the evaluation of new macromolecular cryoprotectants. *Biomacromolecules.* 2020;21(7):2864–2873.

**241**. Liu Y, Xu X, Ma X, Martin-Rendon E, Watt S, Cui Z. Cryopreservation of human bone marrow-derived mesenchymal stem cells with reduced dimethylsulfoxide and well-defined freezing solutions. *Biotechnol Prog.* 2010;26(6):1635–1643.

**242**. Galeano Niño JL, Kwan RYQ, Weninger W, Biro M. Antigen-specific T cells fully conserve antitumour function following cryopreservation. *Immunol Cell Biol.* 2016;94(4):411–418.

**243**. Pasley S, Zylberberg C, Matosevic S. Natural killer-92 cells maintain cytotoxic activity after long-term cryopreservation in novel DMSO-free media. *Immunol Lett.* 2017;192:35–41.

**244**. Wu L, Martin T, Li Y, et al. Cell aggregation in thawed haematopoietic stem cell products visualised using micro-flow imaging. *Transfus Med.* 2012;22(3):218–220.

**245**. Mathaes R, Hildebrandt C, Winter G, Engert J, Besheer A. Quality control of protein crystal suspensions using microflow imaging and flow cytometry. *J Pharm Sci.* 2013;102(10):3860–3866.

**246**. Hildebrandt C, Mathaes R, Saedler R, Winter G. Origin of aggregate formation in antibody crystal suspensions containing PEG. *J Pharm Sci.* 2016;105(3):1059–1065.

**247**. Wang B, Friess W. Lipid-coated mannitol core microparticles for sustained release of protein. *Eur J Pharm Biopharm.* 2018;128:91–97.

**248**. Li T, Chandrashekar A, Beig A, et al. Characterization of attributes and in vitro performance of exenatide-loaded PLGA long-acting release microspheres. *Eur J Pharm Biopharm.* 2021;158:401–409.

**249**. Lengyel M, Kállai-Szabó N, Antal V, Laki AJ, Antal I. Microparticles, microspheres, and microcapsules for advanced drug delivery. *Sci Pharm.* 2019;87(3):20.

**250**. Carpenter JF, Randolph TW, Jiskoot W, et al. Overlooking subvisible particles in therapeutic protein products: gaps that may compromise product quality. *J Pharm Sci.* 2009;98(4):1201–1205.

**251**. Ayuso E, Mingozzi F, Bosch F. Production, purification and characterization of adeno-associated vectors. *Curr Gene Ther.* 2010;10(6):423–436.

**252**. Cattaneo R, Miest T, Shashkova EV, Barry MA. Reprogrammed viruses as cancer therapeutics: targeted, armed and shielded. *Nat Rev Microbiol.* 2008;6(7):529–540.

**253**. Modrow S, Falke D, Truyen U, Schätzl H. *Molekulare Virologie, 3rd ed.* Spektrum Akademischer Verlag; 2010.

**254**. Hastie E, Grdzelishvili VZ. Vesicular stomatitis virus as a flexible platform for oncolytic virotherapy against cancer. *J Gen Virol.* 2012;93(Pt 12):2529–2545.

**255**. Muik A, Dold C, Geiß Y, et al. Semireplication-competent vesicular stomatitis virus as a novel platform for oncolytic virotherapy. *J Mol Med (Berl).* 2012;90(8):959–970.

**256**. Nakanishi M, Otsu M. Development of Sendai virus vectors and their potential applications in gene therapy and regenerative medicine. *Curr Gene Ther.* 2012;12(5):410–416.

**257**. Daikoku E, Morita C, Kohno T, Sano K. Analysis of morphology and infectivity of measles virus particles. *Bull Osaka Med Coll.* 2007;53(2):107–114.

**258**. Gagnon P, Goricar B, Mencin N, et al. Multiple-monitor HPLC assays for rapid process development, in-process monitoring, and validation of AAV production and purification. *Pharmaceutics.* 2021;13(1):113.

**259**. Subramanian S, Maurer AC, Bator CM, et al. Filling Adeno-Associated Virus capsids: estimating success by cryo-electron microscopy. *Hum Gene Ther.* 2019;30(12):1449–1460.

**260**. Kumru OS, Wang Y, Gombotz CWR, et al. Physical characterization and stabilization of a Lentiviral vector against adsorption and freeze-thaw. *J Pharm Sci.* 2018;107(11):2764–2774.

**261**. Perry C, Rayat ACME. Lentiviral vector bioprocessing. *Viruses.* 2021;13(2):268.

**262**. Cole L, Fernandes D, Hussain MT, Kaszuba M, Stenson J, Markova N. Characterization of recombinant Adeno-Associated Viruses (rAAVs) for gene therapy using orthogonal techniques. *Pharmaceutics.* 2021;13(4):586.

**263**. Wyatt Technology Corporation. Adenovirus Particle Characterization. https://wyattfiles.s3-us-west-2.amazonaws.com/literature/app-notes/fff-mals/adenovirus.pdf. Accessed July 15, 2021.

**264**. Hansen E, Lee K, Melotti S, et al. 709. Characterization of Nanoparticles in Lentiviral Vector Preparations. *Mol Ther.* 2016;24:S280.

**265**. Kumru OS, Joshi SB, Thapa P, et al. Characterization of an oncolytic Herpes Simplex Virus drug candidate. *J Pharm Sci.* 2015;104(2):485–494.

**266**. Heider S, Muzard J, Zaruba M, Metzner C. Integrated method for purification and single-particle characterization of Lentiviral vector systems by size exclusion chromatography and tunable resistive pulse sensing. *Mol Biotechnol.* 2017;59(7):251–259.

**267**. Transfiguracion J, Jaalouk DE, Ghani K, Galipeau J, Kamen A. Size-exclusion chromatography purification of high-titer vesicular stomatitis virus G glycoprotein-pseudotyped retrovectors for cell and gene therapy applications. *Hum Gene Ther.* 2003;14(12):1139–1153.